Fall 2014

Carbon dioxide - heavy oil systems: thermodynamics, transport and interfacial stability

Truynh Quoc My Duy Tran

Department: Chemical and Biochemical Engineering

CARBON DIOXIDE - HEAVY OIL SYSTEMS: THERMODYNAMICS, TRANSPORT AND INTERFACIAL STABILITY

by

TRUYNH QUOC MY DUY TRAN

A DISSERTATION

Presented to the Faculty of the Graduate School of the

MISSOURI UNIVERSITY OF SCIENCE AND TECHNOLOGY

In Partial Fulfillment of the Requirements for the Degree

DOCTOR OF PHILOSOPHY

in

CHEMICAL ENGINEERING

2014

Approved by

Parthasakha Neogi, advisor
Muthanna H. Al-Dahhan
Baojun Bai
Kakkattukuzhy M. Isaac
Joontaek Park

ABSTRACT

Conventional oil recovery leaves behind around 67% of original oil in place for light oils and all of it for heavy oils. The carbon dioxide flooding process is the cheapest among the recovery methods for the next stage. The interest here lies in recovering heavy oil. When CO_2 dissolves in oil, it increases the volume of oil, squeezes it out of narrow capillaries and the viscosity of oil drops by up to an order of magnitude. Starting with the available data with and without CO_2 in heavy oil, the free volume theory is used to predict these physical properties. Specific volume CO_2 in the solution is obtained from the swelling data. The viscosity data show us how to obtain the free volumes of CO_2 in oil and hence allow prediction of the diffusivity of CO_2. Separately, an analysis of the displacement process has been undertaken in a single cylindrical pore ~ 1 μm in diameter where the disjoining pressure is included and added to the Laplace pressure, besides the correlations obtained earlier. Numerical solutions have been obtained to provide the results: profile shapes, capillary numbers, and the thickness of thin oil film left behind the drive and net mass transfer rates across the interface. Finally, the viscosity of heavy crude is much higher than the viscosity of CO_2 because of which the displacement process can be unstable leading to fingering or channeling. Linear stability analysis of the displacement process which is that of immiscible displacement but includes mass transfer has been investigated. We are able to provide results that lead to a stabilizing effect overcomes a large destabilizing effect of the adverse mobility ratio. The results show that in the limit that the solubility of CO_2 in oil drops to zero, the above window of instability becomes infinite.

ACKNOWLEDGMENTS

First, I am indebted to Dr. Parthasakha Neogi, my advisor, in a great measure, for teaching me to reason and experiment in natural philosophy. I would like to especially thank Dr. Neogi for his idea, patience, encouragement, and insightful as well as incisive feedback, without him this dissertation would not be possible.

Second, I would like to thank Dr. Muthanna Al Dahhan, Dr. Baojun Bai, Dr. Kakkattukuzhy M. Isaac and Dr. Joontaek Park, my committee members, for their timely feedback, advice and continuing support during my research project.

Third, I would like to thank the faculty, staff and friends from Chemical and Biochemical Engineering Department at Missouri S&T. I would like to thank them for their assistance and cooperation throughout the time I have been in Rolla-MO. Moreover, I need to express my great gratitude to brother (Dr. Thu Tran) who has supported and encouraged me in countless ways during my academic years.

In addition, I would love to thank my parents and my beloved wife, Linh, for their unconditional love, support and understanding.

All of you have made my academic pursuit more enjoyable and rewarding.

Finally, I would love to dedicate this work to my professor: Dr. Parthasakha Neogi.

TABLE OF CONTENTS

Page

ABSTRACT iii

ACKNOWLEDGMENTS iv

LIST OF ILLUSTRATIONS vii

LIST OF TABLES x

SECTION

1. INTRODUCTION 1

    1.1. PRIMARY RECOVERY PROCESS 1

    1.2. SECONDARY RECOVERY PROCESS 2

    1.3. LIMITS ON RECOVERY 2

        1.3.1. Wettability 2

        1.3.2. Interfacial Tension And Capillary Pressure 4

        1.3.3. Mobility Ratio 5

    1.4. ENHANCED OIL RECOVERY(EOR) PROCESSES 5

        1.4.1. Thermal Recovery Process 6

        1.4.2. Chemical Recovery Process 7

        1.4.3. CO_2 Miscible/Immiscible Process 7

    1.5. PRESENT WORK 9

2. FREE VOLUMES ESTIMATES OF THERMODYNAMICS AND TRANSPORT PROPERTIES OF HEAVY OIL WITH CO_2 11

    2.1. INTRODUCTION 11

    2.2. FORMULATION 16

    2.3. COMPARISON WITH EXPERIMENT WITH NO CO_2 18

    2.4. COMPARISON WITH EXPERIMENTS WITH CO_2 22

    2.5. DIFFUSION OF CO_2 IN OIL 33

    2.6. RESULTS AND DISCUSSION 35

3. A SINGLE PORE MODEL FOR DISPLACEMENT OF HEAVY CRUDE OIL WITH CO_2 39

    3.1. INTRODUCTION 39

3.2. FORMULATION 45
3.3. RESULTS AND DISCUSSION 49
4. STABILITY OF CO_2 DISPLACEMENT OF AN IMMISCIBLE HEAVY OIL IN A RESERVOIR 60
4.1. INTRODUCTION 60
4.2. BASE CASE 61
4.3. STABILITY 65
4.4. RESULTS AND DISCUSSION 70
5. CONCLUSION AND RECOMMENDATION 78
APPENDIX 80
BIBLIOGRAPHY 82
VITA 88

LIST OF ILLUSTRATIONS

Figure Page

1.1. Wettability of oil-water-solid system 3

1.2. Oil trapped in pore 5

1.3. Immiscible CO_2 flooding of single process 8

2.1. Scaled densities, Eq. (2.10), have been plotted against pressures (gage) at three different temperatures: triangles at 75°F, diamonds at 140°F and squares at 200°F. 18

2.2. Intercepts from Figure 2.1 have been plotted against temperature 19

2.3. Viscosity μ over the reference viscosity μ′ is plotted as a function of (p-1) atm at 75°F. 20

2.4. The fit to the data at 140°F is shown. 21

2.5. The fit to the data at 200°F is shown. 21

2.6. Solubility of CO_2 (scft/barrel) in oil shown against pressure: triangles at 75°F, diamonds at 140°F and squares at 200°F. 22

2.7. The natural logarithm of Henry's law constant H psi/ (scft/bbl) has been plotted against 1/T where the temperature is in °R.…….. 23

2.8. Swelling factor (SF) has been plotted against the solubility R_s 25

2.9. The calculated values of volume fraction of CO_2 in oil using Eq. (2.27) have been plotted against solubility S 27

2.10. Surface tension data from Rojas and Ali [1988] at 75°F are shown against p_{CO_2} ... 29

2.11. Calculated values of $f_T - f$ 31

2.12. The values of $g - f$ calculated from Eq. (2.30) are shown as functions of p_{CO_2} 32

2.13. The values of $g - f$ calculated from Figure 2.12 have been plotted against $T - T^*$ Eq. (2.33) shows the fitted results.. 33

2.14. Diffusivities have been shown for three temperatures as functions of p_{CO_2} 34

3.1. Fluid *B* is being displaced by fluid *A*. 41

3.2. Using coordinates (say affixed to the nose of the meniscus), it is possible to say that for steady displacement, no dissolved CO_2 would have reached the station downstream, all of the liquid upstream would be saturated and if there is zero shear at the liquid-gas interface then the velocity in the liquid would be plug flow at U backwards 44

3.3. The vector diagram of the velocity field is shown..... 46

3.4. Profiles of the meniscus at Ca = 1.02×10^{-4} and R = 1 μm. 49

3.5. Dimensionless centerline pressure at $Ca = 1.02 \times 10^{-4}$ and R = 1 μm at different times 50

3.6. Dimensionless pressure at the origin at different times 51

3.7. Bold line is the Bretherton result, Eq. (3.1) and the diamonds are results obtained numerically..... 52

3.8. Disjoining pressure of Eq. (3.4) using constants that follow Eq.(3.4) have been plotted for a non-wetting (bold) and for a wetting (dashed) case 53

3.9. Film thicknesses are shown as a function of capillary numbers when disjoining pressures are included. 53

3.10. Film profiles have been shown for $Ca = 1.1037 \times 10^{-4}$, for the non-wetting (a) and the wetting (b) cases. 55

3.11. Effect of mass transfer without the inclusion of disjoining pressures is shown 56

3.12. Mass transferred have been shown differently to illustrate that a saturation is reached. 57

3.13. The decrease in capillary numbers Ca on including mass transfer as a function of Ca when the mass transfer is not included have been shown. 58

4.1. Schematic view of the flooding process and the basic setup for the formulation are shown. 61

4.2. Three different mechanisms due to mass transfer that stabilize the process 72

4.3. (1) represents adverse mobility ratio, the square dotted line (2) is the contribution of mass transfer, the dash- dot line (3) provides variation of viscosity, the round dotted line (4) is the effect of deceleration due to mass transfer, and the dashed line is the total. 74

LIST OF TABLE

Table Page

3.1. Effect of oil viscosity for same inlet velocity of CO_2 in 1μm tube..... 59

1. INTRODUCTION

1.1 PRIMARY RECOVERY PROCESS

Crude oil in reservoirs exists in small pores in the rock formation of limestone and sandstone; these formations are porous. During the initial stage of oil production, oil flows from the reservoir to the wellbore and rises to the surface by the differential pressure between the reservoir and the surface. Indeed, the pressure in the reservoir is much higher than the bottom hole pressure due to hydrostatic pressure of the ground water and the weight above. At this high pressure, gas is naturally dissolved in oil. The structural conditions of the reservoir and the combination of these fluids, connate water, and gas-oil solution provides the driving force to move the oil into the wellbore. Over time, the natural pressure of the reservoir is not sufficient to overcome the flow resistance of the formation to force the oil to the surface and the differential pressure declines. In order to increase the differential pressure or decrease the bottom hole pressure of the production well to maintain the oil production to a desired rate, some kind of pumping equipment is needed. The term of primary recovery is defined by American Petroleum Institute (API) as the production of oil, gas or the combination by naturally occurring forces, physical or mechanical pumping methods. The performance of the reservoir that controls by the natural reservoir energy depends on the reservoir type. They can be grouped into categories based on the principal source of reservoir energy available for oil production are solution gas drive, gravity drainage, gas cap expansion, and natural water drive. However, the primary recovery approaches reach their limitation if the oil production rates are insufficient to economically justify the profitable to continue operation [Muskat, 1949].

1.2 SECONDARY RECOVERY PROCESS

The secondary recovery is implemented to recover the residual oil in the reservoir after the primary recovery can get only 10-30% of original oil in place. Most common methods are water flooding and gas injection. Brine is injected to the injection wells to displace oil toward production wells. Waterflooding is efficient if the oil is a light oil or high API. Gas injection during the secondary process is either into a gas cap to maintain the reservoir pressure and gas cap expansion. A fundamental knowledge of water-oil flow properties of reservoir rock is required to understand the waterflood performance. These are generally grouped into two main types: first, properties of the reservoir rock alone, such as porosity, permeability, pore size distribution, and surface area, and second, rock-fluid properties such as capillary pressure and relative permeability characteristics. The evaluation, performance and most aspects of waterflooding are known [Craig, 1971]. No matter how hard one tries to improve efficiency and production with the present technologies, 2/3 of original oil in place (OOIP) is left in the reservoir after the primary and secondary recoveries.

1.3 LIMITS ON RECOVERY

There are several aspects associated with less efficient displacement of oil in porous media such as wettability, interfacial tension, capillary pressure and mobility ratio in the reservoir. We look at these in brief.

1.3.1 Wettability. Wettability can be defined as the tendency of one fluid to spread on or adhere to a solid surface in the presence of the other immiscible fluid [Craig, 1971]. In displacing oil in porous media, one will consider solid surface as the

reservoir rock and water, oil and gas as the fluids. Figure 1.1 illustrates the wettability of oil-water-solid system. Young-Dupre's equation for surface energies in such a system is as follow:

$$\gamma_{SO} - \gamma_{WS} = \gamma\cos\lambda \qquad (1.1)$$

where γ_{SO} is interfacial tension between oil and solid, γ_{WS} is interfacial tension between water and solid, γ is interfacial tension between oil and water and λ is the contact angle at the oil-water-solid interface measured through the water phase.

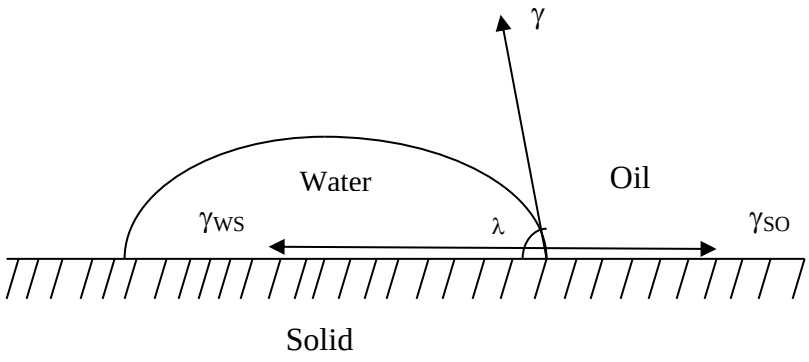

Figure 1.1. Wettability of oil-water-solid system [Craig, 1971].

Contact angle λ is an important parameter in determining rock wettability. If contact angles are less than 90^o, the rock is preferentially water-wet, and if the contact angles are greater than 90^o, the rock is preferentially oil-wet. In addition, contact angles of zero and 180^o are considered strongly water-wet and strongly oil-wet, respectively. Intermediate wet is at contact angles near 90^o. Not all the reservoir rocks are water -wet because organic compounds in the reservoir are absorbed by the rock surfaces and make

the rock surfaces oil – wet. When the reservoir rock is preferentially oil – wet, it is more difficult to dislodge the oil from the pore as oil tries to spread on the rock surfaces.

1.3.2 Interfacial Tension and Capillary Pressure. Capillary pressure in porous media is the pressure difference existing across the interface separating two immiscible fluids. One of which preferentially wets the surface of the rock in reference to the other. Capillary pressure can be expressed as the pressure in the nonwetting phase minus the pressure in the wetting phase [Craig, 1971; Melrose and Brandner, 1974].

$$P_C = P_O - P_W \tag{1.2}$$

where P_C is the capillary pressure, P_W is the pressure in the brine phase, P_O is the pressure in the oil phase. Let us consider an irregular pore containing a blob of residual oil as in Figure 1.2. The pore size is small about 1 micrometer so that the interfacial tension forces between the oil and brine are considered to be large. When we look from right to left, the pressure in the oil blob increases across the interface by an amount which is the product of interfacial tension and the curvature of the interface. Following Young – Laplace's equation:

$$P_O - P_W = -2H\gamma \tag{1.3}$$

where H is the mean curvature of oil and brine. The pressure is constant in the oil blob because of that the oil blob is not able to move. Again, at the interface across the oil blob and brine, there is pressure drop; yet still the oil blob does not move because all forces are balanced even though there is a net pressure drop across the blob [Stegemeier, 1977; Slattery, 1974]. This situation takes place when enough amount of oil has been displaced; the continuity of oil phase no longer exists in the reservoir. That is, the oil volume fraction falls below the percolation point [Larson et al. 1981; Helba et al. 1992].

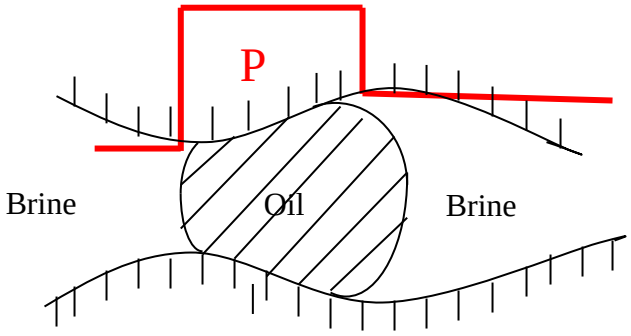

Figure 1.2. Oil trapped in pore.

1.3.3 Mobility Ratio. Mobility ratio is defined as

$$M = \frac{Mobility\ of\ displacing\ fluid}{Mobility\ of\ displaced\ fluid} = \frac{n1}{n2} \tag{1.4}$$

where M is the mobility ratio, $n = K/\mu$, K is permeability and μ is the viscosity. If the mobility ratio, M < 1 the displacement process has a better control in sweep efficiency. For water flooding, the viscosity of oil is much larger than that of brine. The problem that results is that the brine penetrates through the oil in form of fingers or discrete streamers to the production wells, behind the trapped oil. This instability process has been shown in experiments and demonstrated theoretically [Chouke et al. 1950].

1.4 ENHANCED OIL RECOVERY (EOR) PROCESSES

EOR processes involve the injection of materials that are not normally present in reservoir. Conventional water flooding is excluded. Natural energy present in the reservoir is increased by the injection fluids and injection processes. Chemical reaction between the injected fluids and the reservoir rock-oil system can create conditions

favorable for oil recovery. The goal of any EOR process is, to mobilize “remaining” oil. Generally, EOR processes can be divided into these categories: thermal, chemical, gas miscible/immiscible and other processes, such as solvent, and microbial [Green, 1998].

1.4.1 Thermal Recovery Process. The goal of thermal recovery method is, to reduce the oil viscosity, to increase the temperature in the reservoir and displace the low viscosity oil to a producing well. Three processes are commonly used nowadays: cyclic steam stimulation, steam drive and in-situ combustion. Cyclic steam stimulation is a single well method. Steam is injected into a production well in an oil reservoir. The well is then closed in for sometimes to allow heat dissipation to reduce the viscosity of the oil. This oil is next produced through the same well. This process is repeated until the production rate of oil is too low. Production by this method is very good for reservoirs containing oil with high viscosity. In steam drive, steam quality of ±80% is injected through injection wells of a heavy oil reservoir to reduce oil viscosity, oil swelling and steam-vapor drive, making it easier for the steam to push the oil toward production well. A major issue with steam drive processes is that condensation happens at the displacement front decreasing the displacement velocities over injection velocities that go forwards making the displacement stable [Miller, 1975]. In in-situ combustion, heat is generated in the reservoir by combustion. The combustion may use electric heater to start the process then oxygen or air continuously injected to move the combustion zone through the reservoir toward production wells. This method is difficult to control because if the combustion front for any reason is weakened or ceases, the process is lost [Green, 1998].

1.4.2 Chemical Recovery Process. All chemical processes aim to reduce the capillary forces that have trapped the residual oil in porous medium and increase oil production. They are also aimed at reducing the mobility ratio either by itself or in conjunction with the first effect. These include alkaline, surfactants, polymer, alkaline-surfactant, surfactant- polymer and foam. In surfactant-polymer process, a micellar solution containing a surfactant is injected to the injection well. The micellar slug is designed to have an ultralow interfacial tension with the oil phase. Then, polymer solutions of viscosity higher than that of the oil are injected to produce good sweep and eliminate fingering [Stegemeier, 1977]. The surfactant process is complex technologically yet it gives rise to low interfacial tension which is an important aspect in improving oil recovery [Foster, 1973, Amaefule and Handy, 1982; Reed and Healy, 1977]. Alkaline flooding gives rise to a reaction with acid components in oil to produce surfactant in-situ [Green, 1998].

1.4.3 CO_2 Miscible/Immiscible Process. Miscible process occurs when the injected fluid dissolves in reservoir oil completely at the conditions of pressure and temperature existing in the reservoir. The miscible process is the most effective because the surface tension is zero and the residual oils are mobilized and moved toward the production wells. One process that has been suggested to recover the remaining oil is CO_2 flooding because CO_2 gas requires much lower pressures to achieve miscibility than others. When CO_2 gas contacts with oil, some CO_2 dissolves in oil and some oil evaporates into the gas phase then the miscibility is achieved [Hutchinson, 1961].

Immiscible CO_2 flooding is described in Figure 1.3. CO_2 is injected at injection well. Heavy crude is produced at production well. There is an interface between CO_2 and

heavy crude phases. The pores size in the reservoir is around 1 μm . Arrow indicates the flow direction.

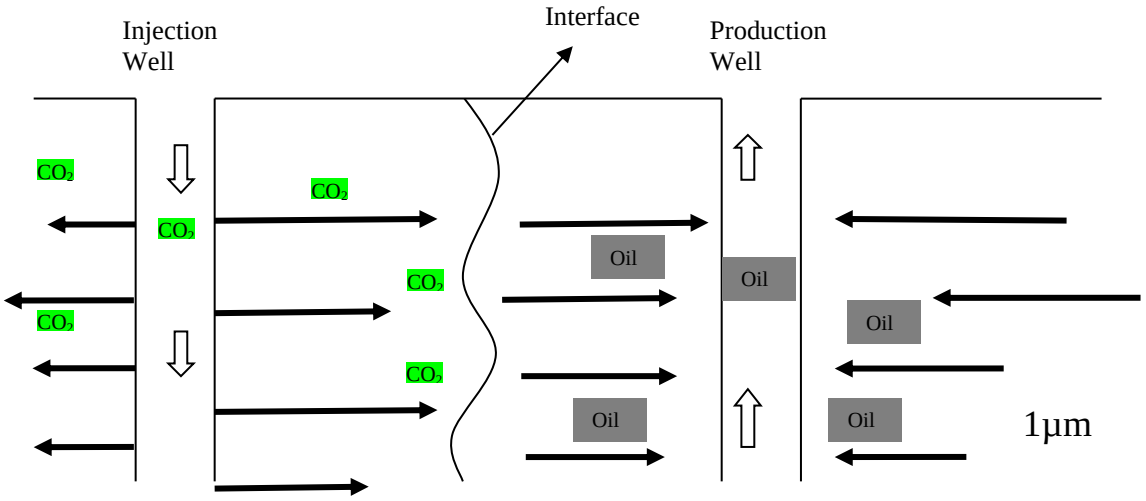

Figure 1.3. Immiscible CO_2 flooding of single process.

Some oils called heavy oils, have very high viscosities, usually specific gravity greater than 0.922. The specific gravity is reported in degree of API gravity, API gravity is computed as (141.5 / SPG) - 131.5, where SPG is the specific gravity of oil at 60^{o}F. Heavy oil has API gravity less than 20^{o}API. API gravity less than 7^o is not recoverable [USGS, 2003]. Heavy oil is very difficult to evaporate and miscibility is not reached. At the interface, CO_2 dissolves in oil; it swells the oil and makes it flow out of narrow pores. In addition, with dissolution of CO_2 the viscosity of heavy oil also decreases by up to an order of magnitude [Welker and Dunlop, 1963; Chung et al. 1988]. In addition, CO_2 process is the cheapest compared to all EOR processes. Moreover, CO_2 flooding is being applied in heavy oil fields [Issever et al. 1993; Paracello et al. 2001; Kang et al. 2013].

Many techniques have been carried out to overcome these difficulties [Hughes and Rao, 2011; Kim et al. 2005].

1.5 PRESENT WORK

It is to be noted that CO_2 flooding is the cheapest process and heavy oils are not recoverable. It would be of great benefit to recover heavy oils with CO_2. There is no such plan given in this proposal but some of the key features are studied. In Section 2 the CO_2- Bartlett heavy oil data [Chung et al. 1988] have been correlated using the free volume theory. A single theory is used to correlate both thermodynamic data and the transport data. The basic feature of the theory is that the interstitial volume among molecules is very low and its change accounts for both thermodynamics and transport. When this volume, called the free volume is large, it is the Arrhenius type of activation energy that becomes controlling. The primary assumption here is that the free volume in heavy oils is small. Some of the thermodynamic data, however, remain energy based. These are the Henry's law constants for solubility and CO_2 – heavy oil surface tension.

In Section 3, the fluid mechanics and mass transfer of CO_2 displacing heavy oil are analyzed in a single model pore of micron sized diameter. The basic model in hydrodynamics is called the Bretherton problem [Bretherton, 1961]. A few important features are analyzed. The first one is how far the dissolved CO_2 penetrates into the oil. The second is the difference between the injected gas velocity and the displacement velocity due to the dissolution. The third is the effect of disjoining pressures in the thin films. Finally, there is the mass transfer itself which is the first time such a study has been conducted for the Bretherton problem. All of these use the physical properties as

found in Section 2, and such physical properties vary strongly with temperature, pressure and CO_2 content.

In Section 4, a linear stability analysis of the displacement process has been analyzed. Average constant permeabilities before and after the front, have been used. Densities have similarly been taken to be constants. Marginal stability case show stabilizing and destabilizing features seen in other analyses, such as in steam flooding [Miller, 1975] and in miscible displacements [Cooney, 1966]. It is seen that CO_2 displacement of heavy oil has some stability, a somewhat surprising conclusion. It is mainly the effect of dissolved stability on viscosity, evaluated from viscosity correlation found in Section 2, that leads to such a result. However, the front is not unconditionally stable and a mushy zone will form there with time.

In Section 5, contains conclusion of this study and recommendation for future research.

2. FREE VOLUME ESTIMATES OF THERMODYNAMIC AND TRANSPORT PROPERTIES OF HEAVY OILS WITH CO_2

2.1 INTRODUCTION

Carbon dioxide is to be used to displace crude oil in reservoirs by effecting miscibility. Even where no miscibility is reached, as in heavy oils, there are still some advantages. When CO_2 dissolves in oil, it increases the volume of oil and squeezes it out of narrow capillaries. Further, the viscosity of oil also decreases at times by an order of magnitude. To quantify the process it is necessary to know the CO_2 solubility, the swelling produced, and the changes in viscosity and diffusivity with the CO_2 content. For instance, we need these for simulation of oil recovery.

There is no available theory that unifies both thermodynamic and transport data in a single model with the exception of the free volume theory which applies when the free volume is low. In addition, most models require a molecular weight of oil, where only a weighted average is available and it is questionable if this weighting will work for oils from different sources, or to different physical properties. We start with the density-pressure-temperature data without CO_2 for heavy oil available in the literature to establish the correlations using the free volume theory and thereby predict the remaining viscosity data. We then interpret the data on swelling by CO_2 which leads us to the volume fraction of CO_2. The viscosity data leads us to the free volumes of CO_2 in oil and allows us to calculate the diffusivities of CO_2.

In all, the energy of solubilization from Henry's law constants, theory of interfacial tension and the diffusivity at infinite dilution using Stokes-Einstein theory are

the only instances where we had to go outside the free volume theory. It is also suggested that the predictions are independent of oil type as long as the oil is sufficiently heavy and the properties are correctly scaled.

Use of CO_2 as a partial solvent to recover crude oil is now a very mature idea [Hutchinson and Braun, 1961]. Standardized procedures are available [Green, 1988]. Even when miscibility is not reached, CO_2 shows some important features. When it dissolves in oil, the oil is seen to swell. The result is that oil gets squeezed out of narrow pores and restricted regions, a very useful property. Further, much of the oil that is available is in the form of heavy oil (specific gravity greater than 0.922, viscosity greater than 100 cP, 1 cP = 1 mPa.s) with very high viscosities that make it extremely difficult to displace. However, with dissolution of CO_2, the viscosity of heavy oil is seen to drop by a factor of up to ten [Welker and Dunlop, 1963; Chung et al. 1988].

Most treatments of data follow Welker and Dunlop [1963] which provides a very successful correlation for swelling. All correlations are empirical [Chung et al. 1988]. From thermodynamic point of view, the solubility and swelling can be calculated using solubility parameters [Prausnitz et al. 1999]. Further refinement has been made by Mulliken and Sandler [1980] by using Peng-Robinson equation of state to obtain the above two quantities. These correlations based on thermodynamics require some data characterizing the crude oil: cubic mean boiling point, Watson's K factor [Watson et al. 1935] (K factor from viscosity is related to specific gravity and boiling point) and solubility parameters that are available in the above references for a number of crudes. Many of those crudes studied are heavy oils. The solubility of CO_2 in brine has also been studied [Chang et al. 1998] as brine exists in all oil fields. A brief review is given below.

Welker and Dunlop's correlation for swelling is

$$SF = 1.0 + 3.5\text{x}10^{-4} R_s \tag{2.1}$$

where *SF* is the swelling factor equal to the volume of CO_2 saturated oil divided by the oil without CO_2 and R_s is simply the solubility of CO_2 in oil at saturation in standard cubic feet per unit barrel of oil only (scft/bbl). Many of the units encountered below are not the ones in usage at present but we continue to use some of those to maintain continuity with the published data. The method for calculation of swelling by using solubility parameters [Prausnitz et al. 1999] is easy to use and is outlined in brief: For the solubility of CO_2 (2) in crude (1)

$$\frac{1}{x_2} = \frac{f^L_{pure2}}{f^G_2} \exp \frac{v^L_2 (\delta_2 - \delta_1)^2 \phi_1^2}{RT} \tag{2.2}$$

where x is the mole fraction, f is the fugacity, v is the specific molar volume, ϕ is the volume fraction, δ is the solubility parameter and RT is the product of universal gas constant and the absolute temperature. The specific volume and solubility parameter of CO_2 are hypothetical quantities that have been calculated and reported by Prausnitz et al [Prausnitz et al. 1999]. The fugacity of CO_2 in the liquid phase as a function of temperature and at 1 atm is also provided in a plot by them. The Poynting pressure correction is

$$f^L_{pure2} = f^L_{pure2\,Ref} . \exp \frac{v^L_2 (p-1)}{RT} \tag{2.3}$$

Fugacity of approximately pure CO_2 where heavy oils are concerned are easy to calculate and are extensively tabulated [Prausnitz et al. 1999]. $\phi_1 = v_1 x_1$ and

$$swelling = \frac{x_2 v^L_2}{x_1 v_1} \tag{2.4}$$

which is the same as R_s when CO_2 is expressed in volumes, and where v_1 is the average partial molar volume of the oil and taken to be that of pure oil. Consequently, the solubility data can be used to calculate the solubility parameter of the oil, or if δ_1 is known then the solubility can be calculated. The main difficulty in following this procedure is that the molecular weight of oil is needed to calculate mole fractions, that is, an appropriately weighted mean. Oil comes from different sources and with different compositions. It is questionable if a single type of weighted mean would be sufficient for all oils, or for all physical properties.

The effect of CO_2 on viscosity has also been studied [Welker and Dunlop, 1963; Chung et al. 1988]. The common method for correlation is the Trouton's rule [Bird, Stewart and Lightfoot, 2002].

$$\mu = A.\exp(3.8T_b / T) \tag{2.5}$$

where the constant A has a molecular interpretation but has also been evaluated by group contribution and suitable activation energy can be used instead of the normal boiling point T_b. Chung et al. [1988] provide one instance of the use of Eq. (2.5) for correlating the viscosities of heavy oils.

Eventually one needs to study mass transfer of CO_2 from the gas phase to the liquid phase. Lake [1988, 1989] has argued that in a displacement process where mass transfer also takes place, it is the molecular diffusivity D which plays the important role and not the larger scale dispersivity. One very important property of both diffusivity and viscosity in such systems is that, they are both strongly concentration dependent. Whereas, the dependence on CO_2 concentration of viscosity can be shown

experimentally, it is very difficult to measure this effect in the experiments on diffusion. Hence some understanding of this effect would be very useful.

The question arises if it is possible to use the same approach to correlate both the thermodynamic and the transport data. This has led the present investigators to look at free volume theories. Very simply the free volume used is the volume fraction not occupied by the impenetrable bodies of the molecules. However, it is very difficult to define [Haward, 1973]. Most investigators take a pragmatic approach to say that the data demand some value for the free volume and look for a value that makes the correlation possible. Free volume theory is ideally suited to study equation of state, and in fact has been used to study transport properties in polymer melts and solids [Haward, 1973; Cohen and Turnbull, 1959; Fujita, 1969; Vrentas and Duda, 1979]. Originally, the theory was used to quantify mobilities where the free volume fraction *f* was small such that the usual treatments with activation energies no longer apply. The assumption holds in solid polymers and melts where it was observed that for these systems the properties became independent of molecular weights of the polymer. It was also observed that some of the parameters used in describing mobilities could be found from the compressibility data. Thus, the studies on polymers [Haward, 1973; Cohen and Turnbull, 1959; Fujita, 1969; Vrentas and Duda, 1979] lead to the possibility that both thermodynamic and transport data for heavy oils can be studied using the free volume theory. The results in some form could also be independent of oil type/source as long as it is heavy.

The free volume theory of viscosity polymer melts shows

$$\mu = RTA_p.\exp(\frac{B_p}{f}) \tag{2.6}$$

The free volume theory for diffusivity polymer melts shows

$$D = RTA_d.\exp(-\frac{B_d}{f_T}) \tag{2.7}$$

2.2 FORMULATION

Consider a volume of oil in reference state: 1 atma, 75°F and no CO_2, which is taken to be V^*. Then by balancing the occupied volumes

$$V^*(1-f^*) = V(1-f) \tag{2.8}$$

For small changes from reference state

$$f = f^* + f_{10}.(p-1) + f_{01}.(T-T^*) \tag{2.9}$$

here, p is the pressure in atma, and various f's with subscripts are constants with - f_{10} as the compressibility and f_{01} the coefficient of volumetric expansion. The volumes chosen in Eq. (2.8) have equal number of oil molecules, hence in terms of densities ρ and in the absence of CO_2

$$\frac{\rho}{\rho^*} - 1 = -\frac{f_{10}}{1-f^*}.(p-1) - \frac{f_{01}}{1-f^*}.(T-T^*) \tag{2.10}$$

It is possible to rewrite Eq. (2.6) in the form

$$\frac{1}{\ln\frac{\mu'}{\mu}} = \frac{1}{B_p}[\frac{f'^2}{\Delta f} + f'] \tag{2.11}$$

where

$$f = f' + \Delta f \tag{2.12}$$

That is, the prime denotes the new reference and the deviation from it shown with a delta, is due to a single parameter. At fixed temperature, $\Delta f = f_{10}.(p-1)$ from Eq. (2.9) and a straight line is obtained by plotting the left hand side in Eq. (2.11) against 1/ (p-1) since f' is a constant. Similarly, p can be held constant and T varied, and the left hand side of Eq. (2.11) is plotted against 1/(T-T*) since $\Delta f = f_{01}.(T-T^*)$.

In presence of CO_2, the free volume of the mixture

$$f_T = (1-\phi) f + \phi g = f + \phi(g-f) \tag{2.13}$$

where g is the free volume of CO_2 and ϕ is its volume fraction. As emphasized by Vrentas and Duda [1979], the free volumes in liquids when the molecules are small are much larger than that of a solid, as Vrentas and Duda [1979] were looking at diffusion of small molecules through solid polymers. We have extended this concept to very viscous liquids, that is, heavy oil, which is close to a solid. Thus, f_T increases over f. This causes the viscosity to fall. Similarly for diffusivity, it is possible to write Eq. (2.7) in the form

$$\frac{1}{\ln \frac{D_o}{D}} = \frac{1}{B_d}\left[\frac{f^2}{\phi(g-f)} + f\right] \tag{2.14}$$

where D_o is the diffusivity at infinite dilution. Eq. (2.14) is only used to treat isothermal systems, where it will show only concentration effects. It is often assumed that $B_p/B_d = 1$ or $B_p = 1$. Here, B_p is the smallest size of hole necessary for the solvent molecule (a molecule or a segment of a molecule as in polymers) to move into, and B_d is the smallest size of the hole necessary for the solute to move into. Where they have been determined [Fujita, 1969; Vrentas and Duda, 1979] the difference is small and so they are set equal below. Chung et al. [1988] has given tabulated data on densities and viscosities that we use in the next section. It should be kept in mind that the above data with CO_2 are at

saturation. In the section that follows, the various effects of CO_2 on oil, solubility, swelling, changes in viscosity and surface tension, and diffusivity, are analyzed. The unifying theme here is the use of free volume theory which so far has not been used in these systems. The fundamental basis for the thermodynamics of free volume theory [Kirkwood, 1950] and its application in transport [Cohen and Turnbull, 1959] are known.

2.3 COMPARISON WITH EXPERIMENT WITH NO CO_2

The data of Chung et al. [1988] of oil densities without CO_2 versus pressure, using Eq. (2.10). The slopes in Figure 2.1 are $5.758\text{x}10^{-5}$, $6.14314\text{x}10^{-5}$ and $6.2214\text{x}10^{-5}$ at the three temperatures. They are all very close.

Hence, using the average value

$$-\frac{f_{10}}{1-f^*} = 6.041\text{x}10^{-5} \pm 0.163\text{x}10^{-5}\ per\ atm \qquad (2.15)$$

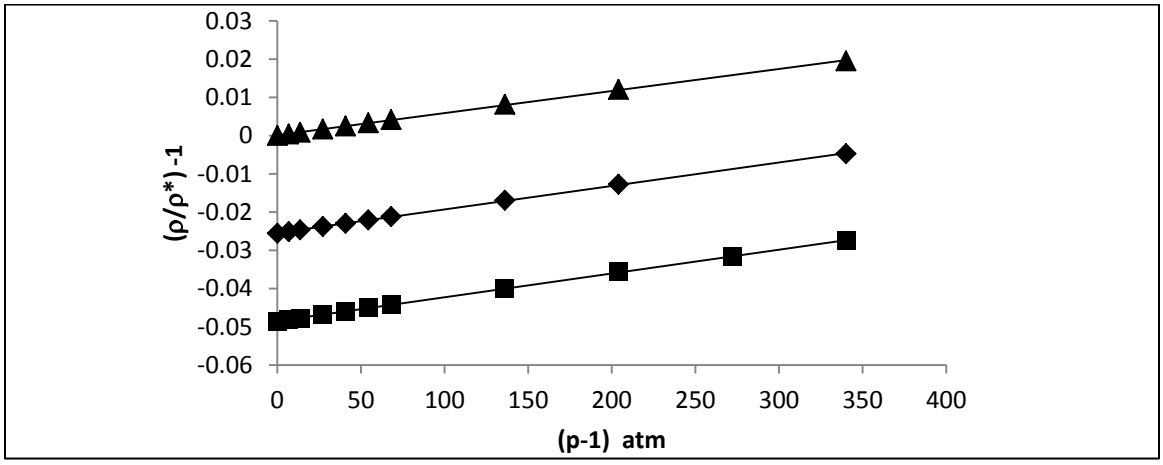

Figure 2.1. Scaled densities, Eq. (2.10), have been plotted against pressures (gage) at three different temperatures: triangles at 75°F, diamonds at 140°F and squares at 200°F. The reference density ρ* is everywhere at 1 atma and 75°F. Data are from Chung et al. [1988].

It shows that the density increases with pressure. The intercept from Figure 2.1, have been plotted against T - T* in Figure 2.2 and the slope gives us

$$\frac{f_{01}}{1-f^*} = 3.891\text{x}10^{-4}\ per\,°F \tag{2.16}$$

showing that density decreases with temperature. Comparing Eqs. (2.15) and (2.16) it can be observed that the pressure effect is smaller than the temperature effect.

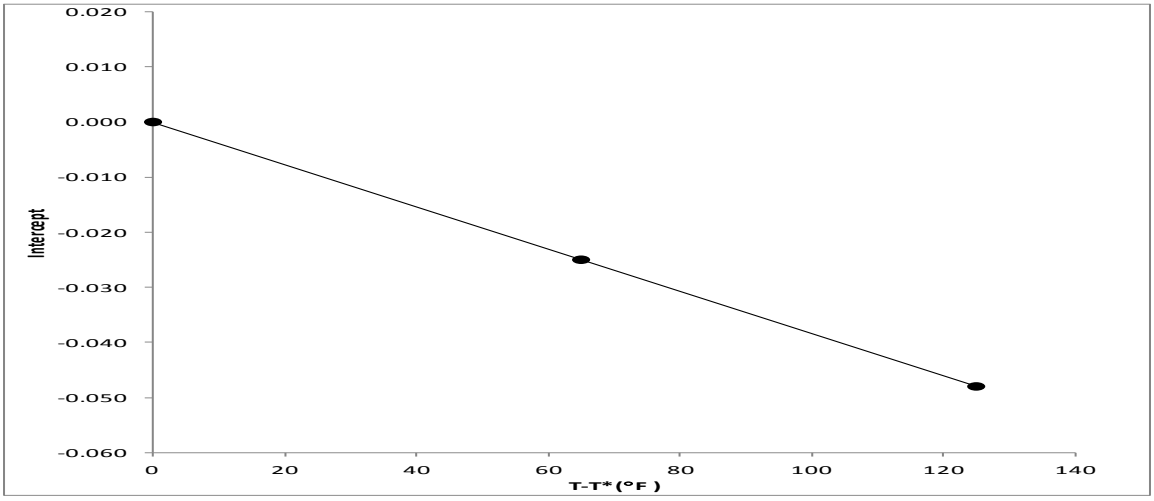

Figure 2.2. Intercepts from Figure 2.1 have been plotted against temperature. The reference temperature T* = 75°F.

From Eq. (2.6), we can write

$$\mu^* = RT^* A_p.\exp(\frac{B_p}{f^*}) \tag{2.17}$$

where the starred quantities are at the reference values of 1 atma, 75°F and no CO_2. For these reference values, the viscosity data of effect of pressure at 75°F were fitted to Eq. (2.11), with $\mu' = \mu^*$ and $f' = f^*$ and $\Delta f = f_{10}.(p-1)$ to get

$$B_p = 1.000 \tag{2.18}$$

$$f^* = 0.02088 \tag{2.19}$$

using non-linear regression. Plot of the fit is shown in Figure 2.3, with a standard deviation of 0.1000. Since all parameters are known, Figure 2.4, and Figure 2.5, show the difference between the predicted and the experimental values. The two agree well at 200°F but not so well at 140°F is because the data at high pressures and those at low pressures appear to follow two different trends. The predicted values tend to favor the data at larger pressures.

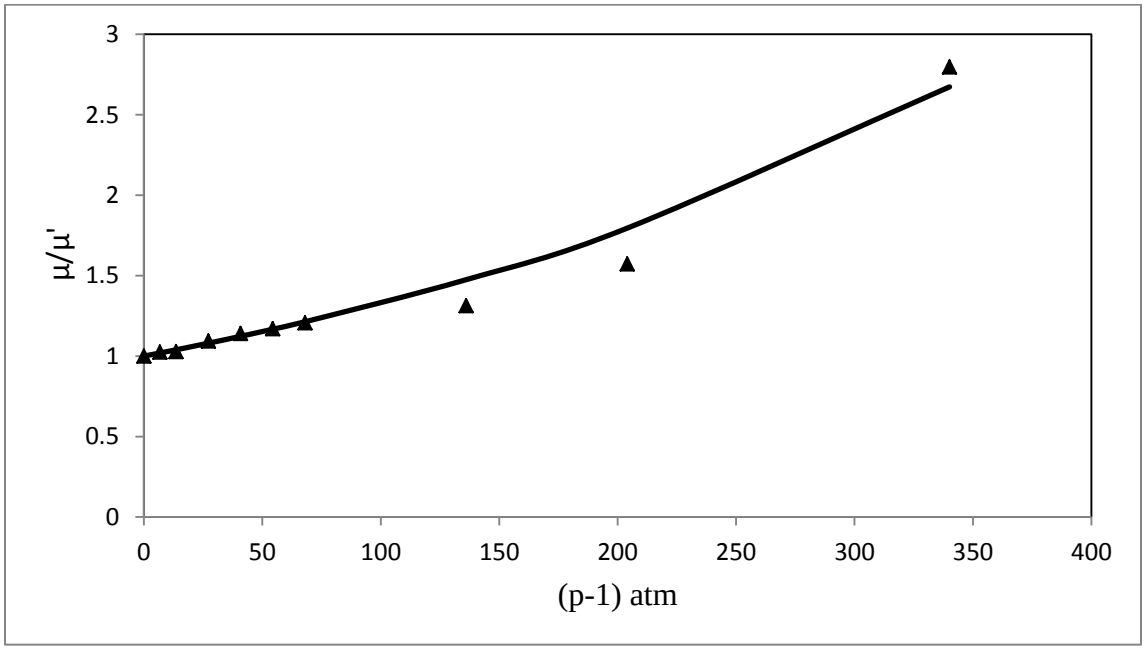

Figure 2.3. Viscosity μ over the reference viscosity μ′ is plotted as a function of (p-1) atm at 75°F. Data are from Chung et al. [1988].

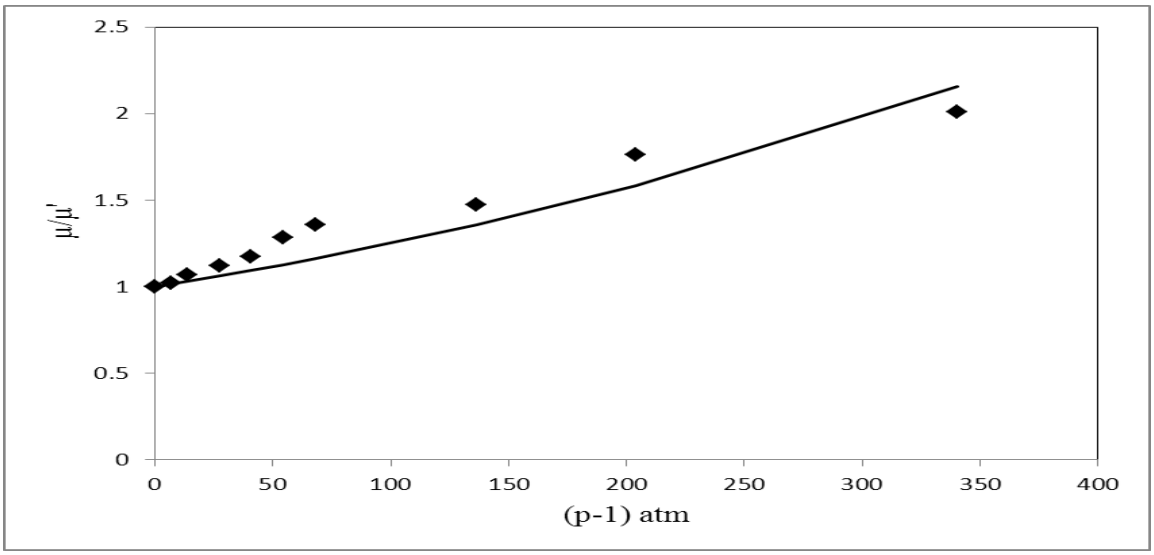

Figure 2.4. The fit to the data at 140°F is shown. The fit appears fractured in the sense the data for small pressures and large pressures cannot be fitted by the same curve. The choice has been for fit at large pressures. There are no adjustable parameters. Data are from Chung et al. [1988].

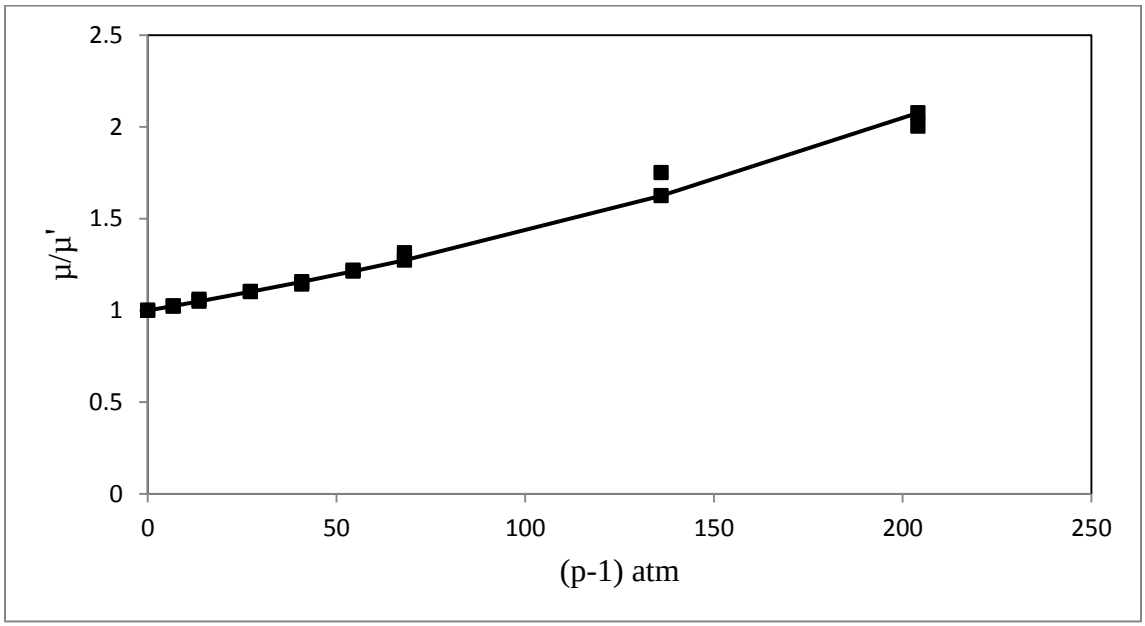

Figure 2.5. The fit to the data at 200°F is shown. There are no adjustable parameters. Data are from Chung et al. [1988].

2.4 COMPARISON WITH EXPERIMENTS WITH CO_2

The solubilities [Chung et al. 1988] have been plotted against pressure in Figure 2.6. In these experiments, the partial pressure of CO_2, that is, p_{CO2}, is the same as the total pressure p. There is an unusual amount of scatter in the high pressure region which is confined to ~ 4000 psia as a result this cluster of data has been omitted. The remaining data also extend to high pressures of up to 2000 psia. It is also clear that after omitting this cluster the remaining data are seen to follow linear Henry's law making it unnecessary to convert pressure to fugacity.

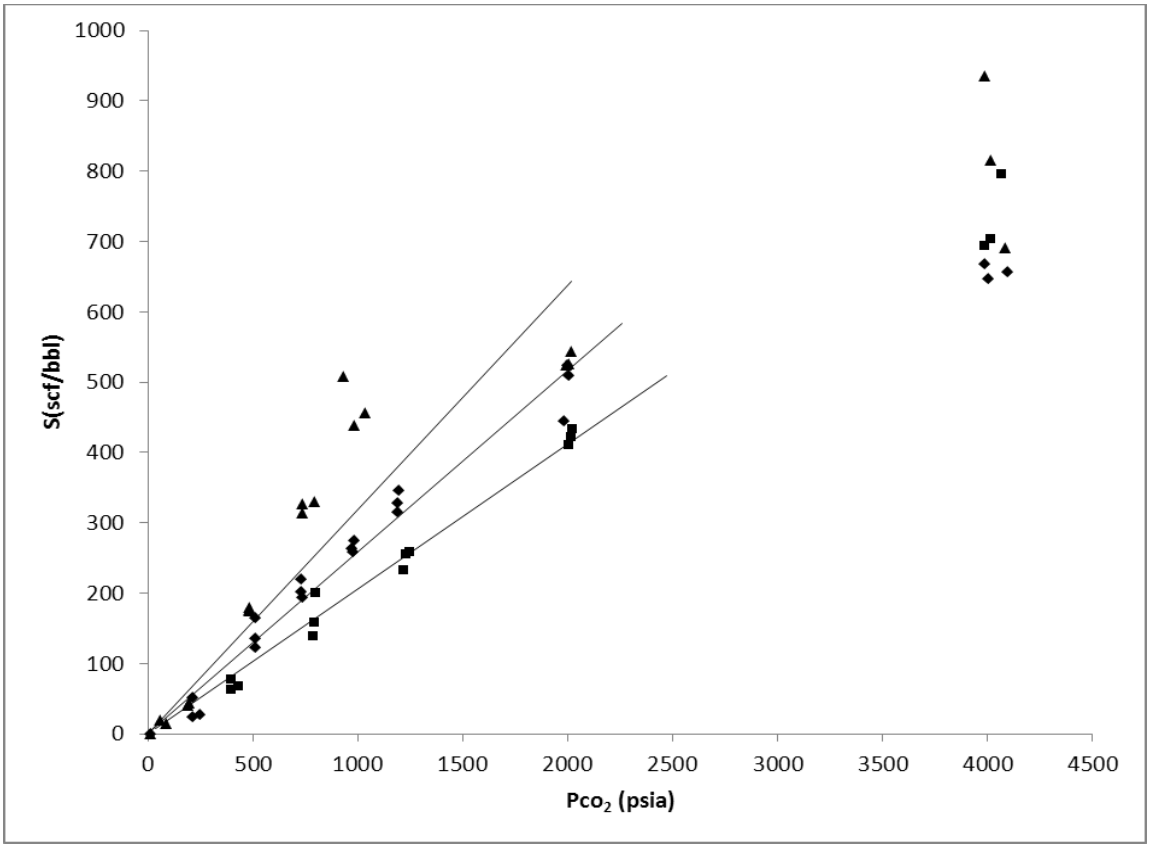

Figure 2.6. Solubility of CO_2 (scft/barrel) in oil shown against pressure: triangles at 75°F, diamonds at 140°F and squares at 200°F. Data are from Chung et al. [1988].

This characteristic feature that Henry law holds even on including the high pressure data has been observed [Prausnitz et al. 1999]. The Henry's law constants *H* are 3.1338, 3.8685 and 4.8473 psi/ (scft/bbl) at 75, 140 and 200ºF, respectively. The standard deviations are 210.7, 25.0 and 17.6 scft/bbl respectively, showing very large scatter at the lowest temperature. In Figure 2.7, the natural logarithm of *H* has been plotted against 1/T. A straight line has been fitted with a standard deviation of 0.0539. The characteristic temperature is seen to be 760.6 ºF (1220.3ºR). The fitting leads to

$$\ln H = -1220.3/T(^{\circ}R) + 3.4135 \qquad (2.20)$$

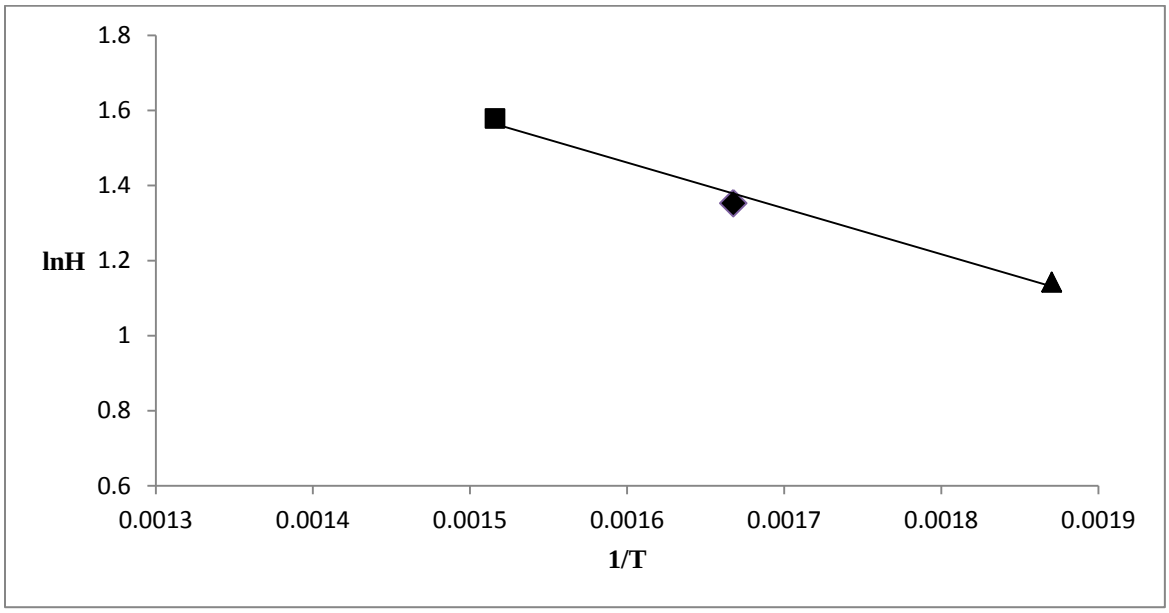

Figure 2.7. The natural logarithm of Henry's law constant H psi/ (scft/bbl) has been plotted against 1/T where the temperature is in °R. The slope of the fitted straight line is 1220.3°R or 760.6°F.

This is the first of the three quantities for which we have to go outside the free volume theory.

The key result in the studies with CO_2 is its solubility (g/cm^3). Two quantities are defined. The first is the swelling factor *SF*. It is

$$SF = \frac{volume\,occupied\,by\,oil\,containing\,CO_2}{\begin{array}{l} volume\,occupied\,by\,the\,same\,mass\,of\ \ oil\,without\,CO_2 \\ at\,1\,atma\,and\,the\,same\,temperature \end{array}} \tag{2.21}$$

SF can be calculated from the data of Chung et al. [1988] :

$$SF = \frac{\rho_1}{\rho - S} \tag{2.22}$$

where ρ is the density of the solution (g/cm^3), S is the solubility of CO_2 (g/cm^3) and ρ_1 is the density of oil (with no CO_2) at the same temperature and 1 atma pressure. Another solubility is defined using volume of oil only (g/cm^3)

$$R_s = \frac{S\rho_1}{\rho - S} = S.SF \tag{2.23}$$

We emphasize the difference between the two solubilities S and R_s is that the volumes used for S is the total volume of solution at that temperature and pressure but that used for R_s is the volume of oil only at 1 atma and the same temperature. When plotted in the form of R_s versus S, the numbers from Chung et al. [1988] agree with the Welker and Dunlop [1963] equation, Eq. (1), as shown in Figure 2.8.

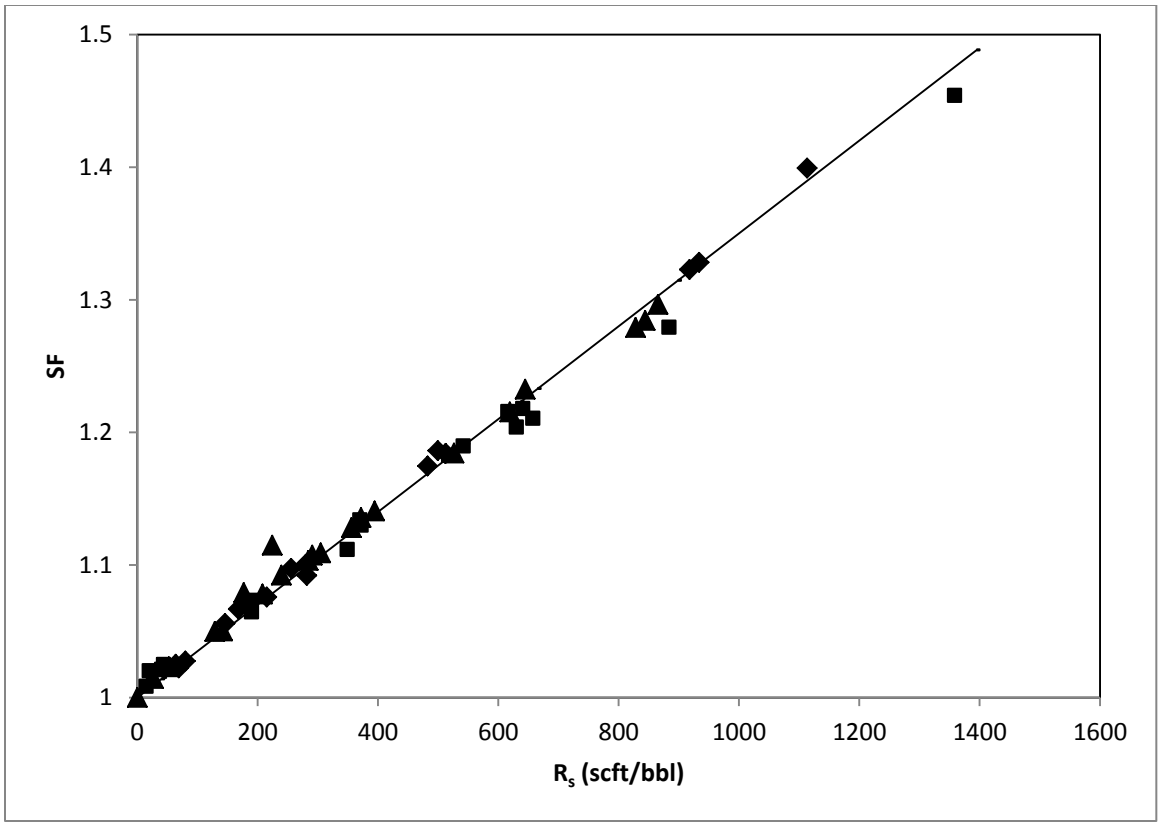

Figure 2.8. Swelling factor (SF) has been plotted against the solubility R_s. The triangles are at 75°F, diamonds at 140° and squares at 200°. Data are from Chung et al. [1988]. The line is the Welker and Dunlop correlation [1963], Eq. (2.1).

Consider now 1 cm^3 of oil containing CO_2. The volume of CO_2 there is ϕ and oil is 1 - ϕ. Further the mass of oil is ρ - S g and mass of CO_2 is S g. Hence, the partial density of oil is (ρ - S)/ (1 - ϕ). Hence,

$$\frac{\rho - S}{(1-\phi)(1-f)} = \rho_{Ho} \tag{2.24}$$

where ρ_{Ho} is the density of oil of hard dimensions (extensive of the concept of impenetrability) only. Similarly,

$$\frac{\rho_1}{(1-f_1)} = \rho_{Ho} \tag{2.25}$$

Combining Eqs. (2.24) and (2.25), and using expansions for the free volume from Eq. (2.9), one has

$$SF = \frac{\rho_1}{\rho - S} = \frac{1 + f_{10}.(p-1)}{1-\phi} \tag{2.26}$$

Eq. (2.26) allows us to calculate ϕ for every set of data from Chung et al. [1988]. Further,

$$\phi = S.v_{CO_2} \tag{2.27}$$

Eqs. (2.1), (2.22) and (2.23) can be combined to write first that

$$SF = 3.5\text{x}10^{-4}.SF.S + 1.0 \tag{2.28}$$

leading next to

$$SF = \frac{1}{1 - 3.5\text{x}10^{-4}.S} \tag{2.29}$$

where S is in scft/bbl. Eq. (2.29) does not contain any results from the free volume theory, but Eq. (2.26) is the free volume theory result. Comparing the two

$$1.06 = v_{CO_2} \tag{2.30}$$

is obtained where the small pressure dependence in Eq. (2.26) is ignored. A change in units has been made from $3.5\text{x}10^{-4}$ bbl/scft to the left hand side in Eq. (2.30) to 1.06 cm^3/g. Calculated values of ϕ from Eq. (2.26) and (2.27) have been plotted against S in

Figure 2.9. The data look remarkably linear and independent of temperature and pressure. The line of slope of 1.06 cm^3/g also fits well.

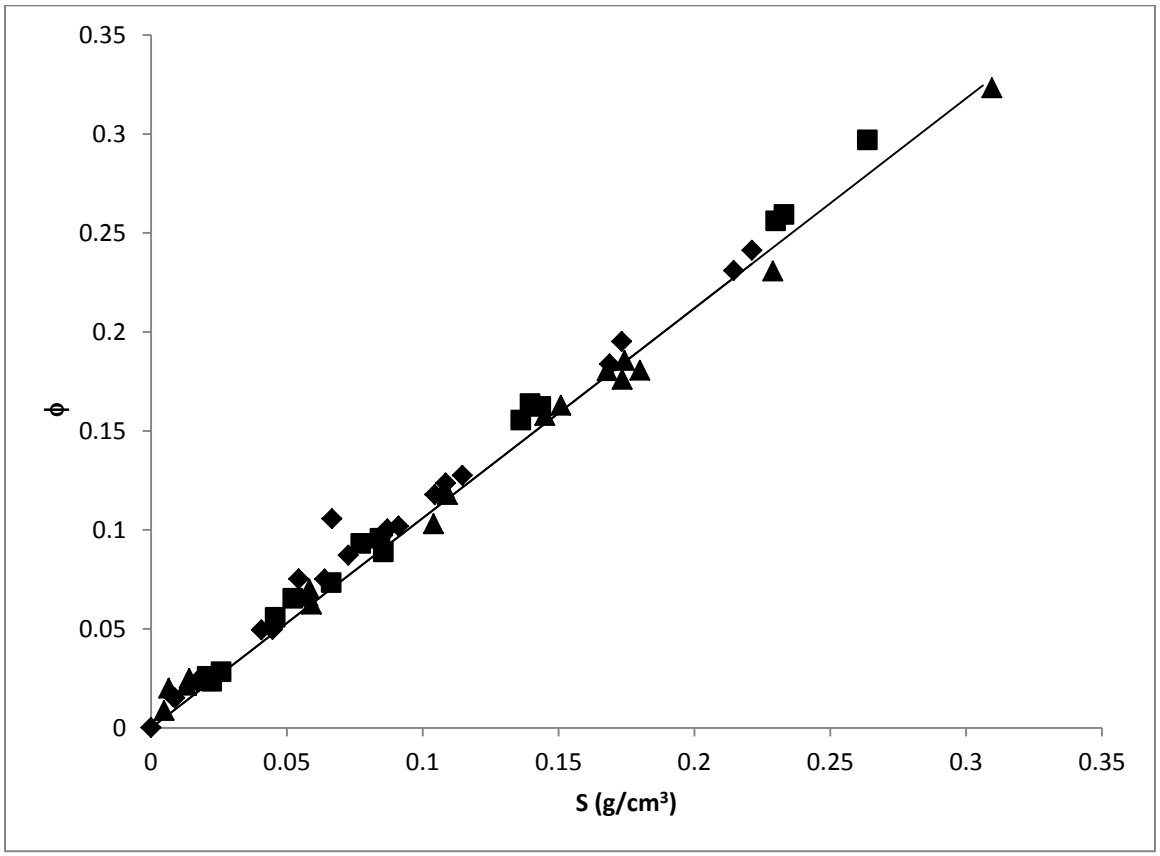

Figure 2.9. The calculated values of volume fraction of CO_2 in oil using Eq. (2.27) have been plotted against solubility S.

The volume fractions, a dimensionless concentration, indicate that the system is by no means dilute in CO_2. From Prausnitz et al. [1999] it could be suggested that the value of v_{CO_2} here should be the same as v_2^L in Eqs. (2.2) - (2.4), the value of which for

CO_2 is 1.25 cm^3/g. Instead of using this last value, some investigators [Kulkarni and Stern, 1983] have suggested the use of the critical volume of CO_2 of v_c = 2.14 cm^3/g, but that appears too high for the present use.

The last thermodynamic quantity needed is the surface tension in presence of CO_2. Rojas and Ali [1988], indicate in their study on immiscible displacement of oil by CO_2, that the decrease of surface tension of oil by CO_2 is a major factor in improved recovery. The thermodynamics of surface tension of a solution is available [Miller and Neogi, 2008]. Its main feature is that the concentration of the solute in the bulk is different from that on the surface, that is, a component can be surface active. The present case contains two new features. In case of CO_2, one difficulty arises that we do not have a state where there is a vapor-liquid interface involving pure CO_2 since not always are we interested in conditions below the critical. Lack of this condition necessitates the use of a surface Henry's law. Another complication is that the molecular weight of oil is not known. As a result lattice theory and volume fractions are used for chemical potentials (instead of mole fractions). The details of the derivation are given in the Appendix. The result is

$$1 = \phi H_s . \exp(\gamma a_2 / RT) + (1-\phi) . \exp[(\gamma - \gamma_1) a_1 / RT] \qquad (2.31)$$

where H_s is the surface Henry's law constant defined by $H_s = \exp[\frac{\mu^{o,s} - \mu^o}{RT}]$ in terms of the two standard state chemical potentials, and γ is the surface tension of the mixture, γ_1 is the surface tension of the pure oil, a_2 and a_1 are the partial molar areas of CO_2 and oil at the surface respectively. The first term on the right hand side in Eq. (2.31) is ϕ_s, the volume fraction of CO_2 at the surface. Eq. (2.31) contains three parameters. The

chemical potentials in the lattice theory have also been approximated for a dilute solution, in keeping with the use of Henry's law and helps to keep the number of parameters down. It has been assumed as well that the partial molar area of the oil is same as that of the pure component = a_1 and the partial molar area of CO_2 at the surface is a constant = a_2. The data and the fitted curve have been shown in Figure 2.10. The fit is quite reasonable with a standard deviation of 1.5658 mN/m. More important, a_2 = 1.56x10^9 cm^2/mol = 25.9 Å^2/molecule.

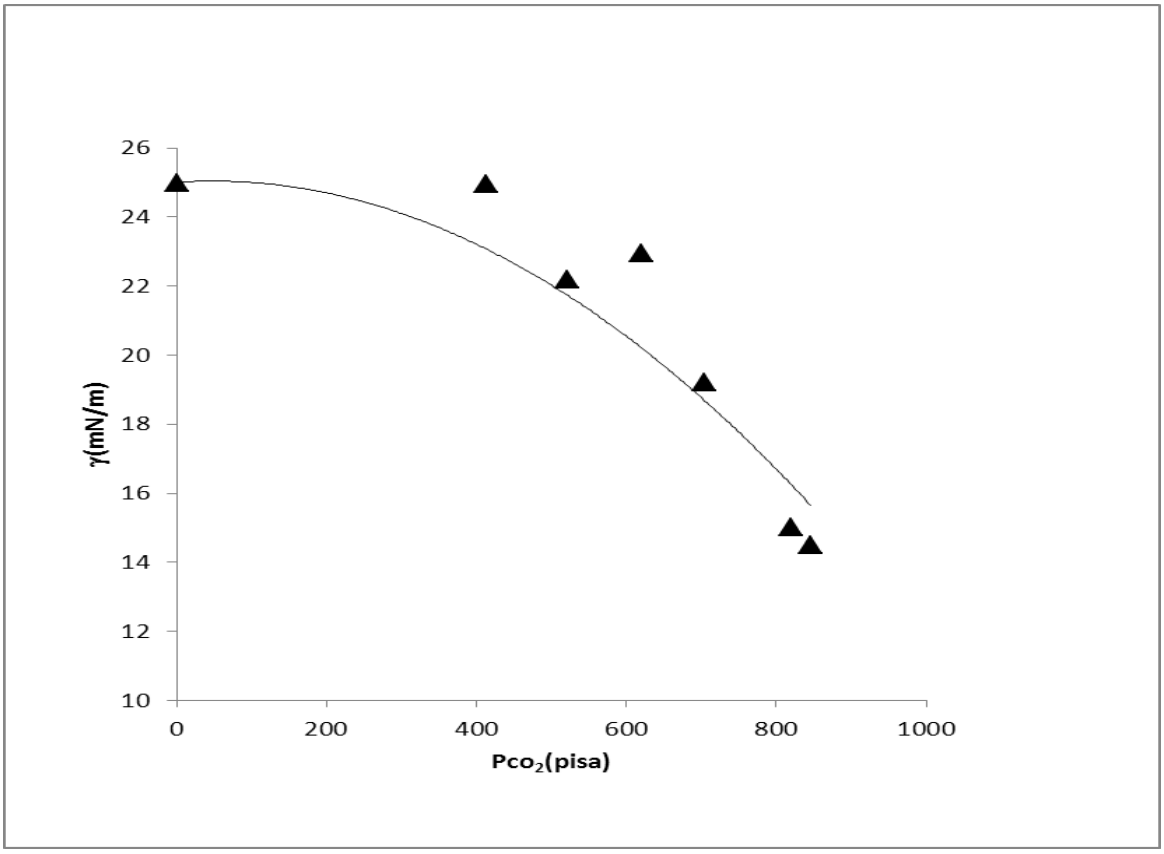

Figure 2.10. Surface tension data from Rojas and Ali [1988] at 75°F are shown against p_{CO_2}. The curve is the fit from Eq. (2.31).

If it is assumed that the CO_2 molecule at the surface is perfectly circular, then its radius works out to 2.87 Å, which compares well with σ = 3.996 Å from the Lennard-Jones potential [Bird, Stewart and Lightfoot, 2002]. Now $a_1 = 1.8\text{x}10^{10}$ cm^2/mol = 298.9 Å^2/molecule represents a radius of 9.7 Å. Obviously, the oil molecule only lies partially on the surface, but is mostly oriented perpendicular to it, that is, assuming that the oil is mainly *n*-alkane. Finally, $H_s = 2.896$. That is, CO_2 is surface active. The data are all at 75°F so no more information can be obtained from these parameters.

Consider now the viscosity in presence of CO_2. From Eq. (2.11) it is possible to get for this case

$$\ln \frac{\mu}{\mu_1} = B_p[\frac{1}{f_T} - \frac{1}{f_1}] \tag{2.32}$$

μ_1 and f_1 are the viscosity and free volume with no CO_2, 1 atma pressure and same temperature. Since the viscosity is lowered in presence of CO_2, it follows from Eq. (2.32) that f_T is higher than f_1.

However, a problem arises with experimental errors in obtaining g from Eq. (2.13). It is necessary to divide one quantity determined from the experimental data by another also determined from the data in the form of $\frac{f_T - f}{\phi}$ to get $g - f$. In the limit that ϕ goes to zero, both the numerator and the denominator are dominated by errors. However, the results for $g - f$ does have a look of constant independent of p_{CO_2}. Because of this we have fitted straight lines through $f_T - f$ versus p_{CO_2} plots that pass through the origins in Figure 2.11. Plots of ϕ versus p_{CO_2} have not been drawn as they are similar to

ϕ versus S as shown in Figure 2.9. Constants values are obtained for $g - f$ as shown in Figure 2.12, along with the calculated numbers.

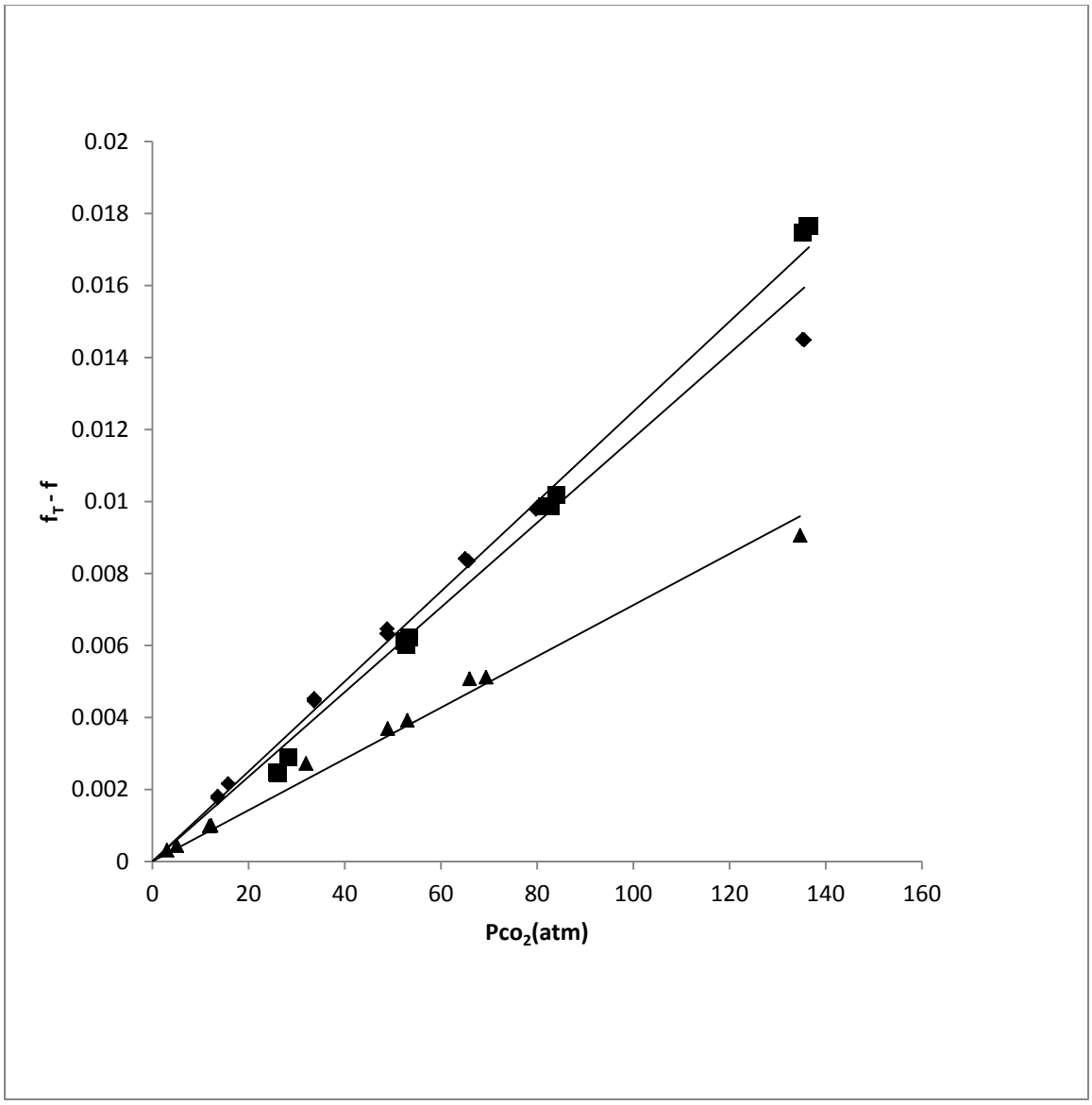

Figure 2.11. Calculated values of $f_T - f$. Using Eq. (2.30), and calculated values of ϕ from Eq. (2.25) have been plotted against p_{CO_2} and straight lines that pass through the origin have been fitted to all. The experimental scatter for a few of these plots are large.

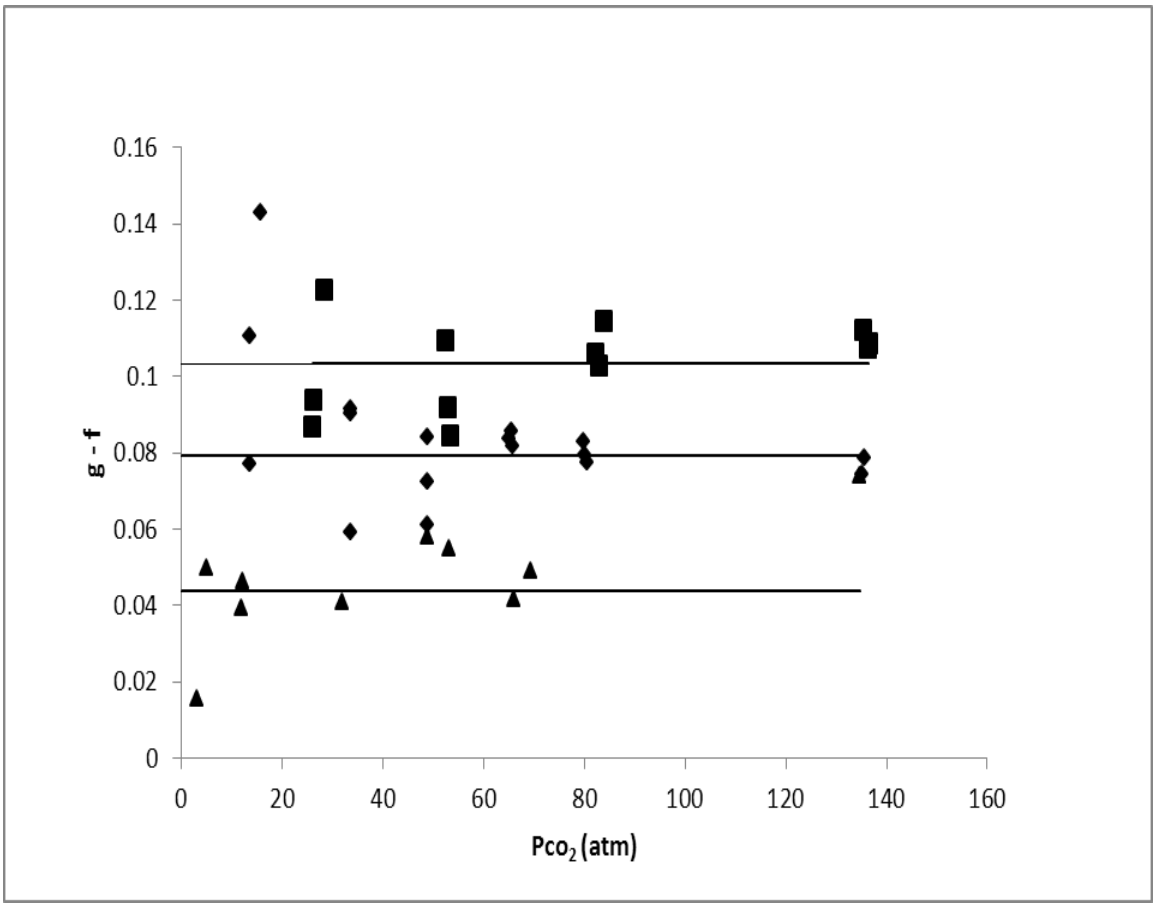

Figure 2.12. The values of g – f calculated from Eq. (2.30) are shown as functions of p_{CO_2} . The horizontal lines have been calculated using the slopes in Figure 2.11. The fit looks reasonable.

In Figure 2.13, g – f values have been plotted against T – T* to get

$$g - f = 4.7816x10^{-4}(T - T^*) + 4.5244x10^{-2} \qquad (2.33)$$

The values of *g* are about twice the values of *f* or more. It is seen that the scatter to constant *g* – *f* at lower pressure in Figure 2.12, are large but appear to be unbiased.

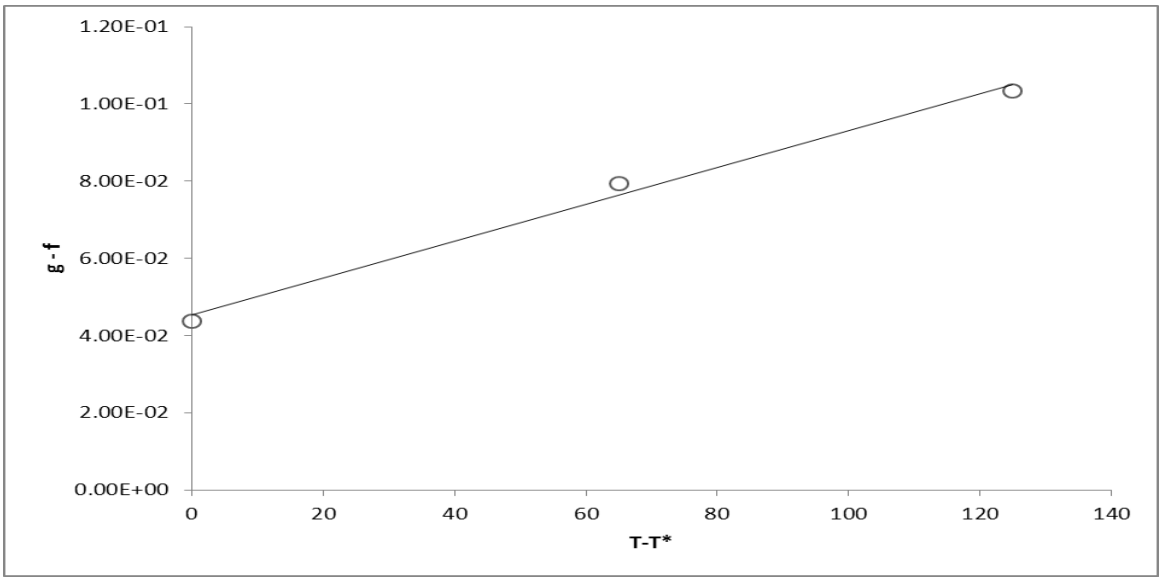

Figure 2.13. The values of g – f calculated from Figure 2.12, have been plotted against T – T*. Eq. (2.33) shows the fitted results.

2.5 DIFFUSION OF CO_2 IN OIL

In Eqs. (2.7) and (2.14), we make the adjustment that the reference diffusivity is at 1 atm and at that temperature which leads to

$$D = D_1 \exp[\frac{B_p}{f_1} - \frac{B_p}{f_T}] \tag{2.34}$$

where it has been assumed that $B_p = B_d$. It still needs D_1 which is taken here to given by Stokes-Einstein equation

$$D_1 = \frac{k_B T}{6\pi\mu_1 a^*} \tag{2.35}$$

where k_B is the Boltzmann constant and a^* is the radius of carbon dioxide molecule, here is set as the Lennard-Jones parameter [Bird, Stewart and Lightfoot, 2002] $\sigma/2$. The results are shown in Figure 2.14.

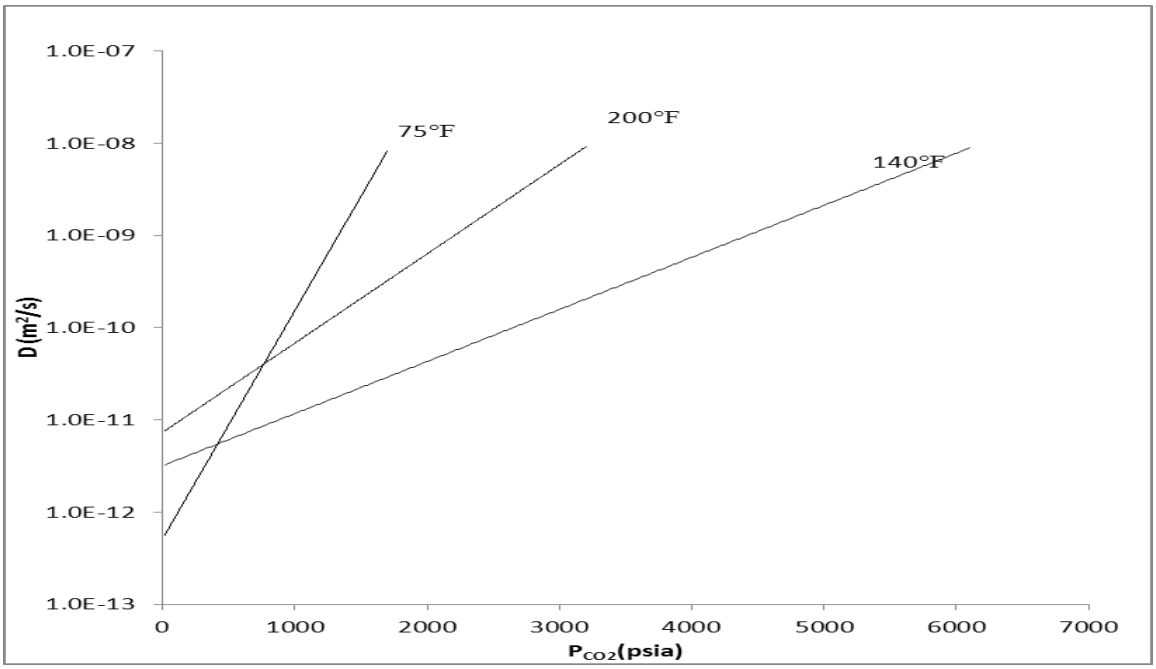

Figure 2.14. Diffusivities have been shown for three temperatures as functions of p_{CO_2}. Eqs. (2.34) and (2.35) have been used.

First, there are many orders of magnitude increase in the values of diffusivities with the pressure of CO_2, and alternatively the concentration. Second, the increase with temperature is not straightforward. At low pressures *D* versus *T* are in sequence but at higher pressures they are out of sequence. At infinite dilution, the diffusivity increases with temperature. Hence, the one with the lowest temperature is the lowest. However, the solubility of CO_2 is highest at the lowest temperature. Thus, with increased CO_2 pressures, the dissolved CO_2 content increases, the free volume and diffusivity increase the fastest at the lowest temperature to overtake the rest. Finally, as the diffusivity is concentration dependent and hence the diffusivities that are measured experimentally [Yang and Gu, 2006(48), (64); Tharanivasan et al. 2006; Yang and Gu, 2008; Zhang et

al. 2000] are averages over the concentration ranges encountered. These results are for light oils where the free volume theory may not apply whether or not the diffusivities are concentration dependent. Crank and Park [1968] have emphasized a few things of importance here. The response to a concentration dependent case and a constant diffusivity case both satisfy the same type of functional dependence, such as a function of time *t*. Thus, it is very difficult to determine if diffusivity is concentration dependent from such data [Kulkarni and Stern, 1983].

Consequently, this form of diffusivity suggested by the free volume theory is very different and poses challenges to both dealing with it theoretically and experimentally. These calculations provide some preview of what they may be.

2.6 RESULTS AND DISCUSSION

The procedure that was followed here was to use established theoretical relations to treat thermodynamic and transport quantities and show that they apply to the present case of CO_2 and heavy oils. The data are all from Chung et al. [1988] with the exception of the data on surface tension which are from Rojas and Ali [1988]. There are about six parameters calculated for the free volume theory and an assumption $B_p = B_d$ is used. The values of the parameters look reasonable and the theory provides meaningful interpretations. The heavy oil analyzed in Figures 2.1 and Figure 2.2, shows constant isothermal compressibility and coefficient of volumetric expansion. The viscosity data of pure oil also fitted to the free volume theory quite well in Figures 2.3, 2.4, and 2.5. It should be emphasized that only in Figure 2.3, were the remaining parameters obtained. All parameters were known from before in Figures 2.4, and 2.5. Hence, the theoretical

values there are predictive. There is also one feature here that is of importance to the free volume theory, namely that the absolute values of free volumes *f* were obtained and used thereafter. This is relatively rare.

For systems containing CO_2, it was found that the solubility followed Henry's law, Figure 2.6. This is not very surprising because CO_2 at high pressures behaves as non-polar compounds, same as the oil. The correlation for the Henry's law constants developed (Figure 2.7), proves useful later in converting pressures of CO_2 to volume fraction dissolved. A derivation based on free volume theory, is shown to lead to Welker and Dunlop [1963] correlation (Figure 2.8) and a coefficient that arises in that correlation is shown to lead to the specific volume of CO_2 in the solution (Figure 2.9). This section of thermodynamic data is completed with analysis of oil-CO_2 surface tension. The data are available only at 75°F. However, as seen in Figure 2.10, the fit appears reasonable and the parameters have been shown to be reasonable. CO_2 appears to be surface active.

The data on viscosity show significant scatter. The data were to be used to determine the free volume *g*, of the dissolved CO_2. It is observed that *g* is considerably larger than *f*, and to the extent that the scatter permits, $g - f$ is seen to be only dependent on temperature. The fact that *g* is larger, is expected for smaller molecules as explained earlier. Various aspects of these difficulties and how they are taken care of are shown in Figures 2.11- 2.13.

One main feature of CO_2 oil recovery process that we need to know is the rate of dissolution of CO_2 in oil. To have a quantitative view of mass transfer it is necessary to have knowledge of the diffusivity. The diffusivities calculated from the free volume theory as shown in Figure 2.14, is very strongly dependent on concentrations. This

suggests that the measured diffusivities are averages and makes it necessary to re-evaluate calculations and methods of measurements.

At two places, scatter in the data has turned out to be large and it is worth commenting on the sources. In Figure 2.6, the data at 4000 psia have been ignored for the scatter. At those very high pressures it is possible that miscibility or near miscible conditions have been reached even though the oil is heavy oil. This could make observations difficult. We also see a lot of scatter in Figure 2.12, and one reason that has been suggested is that the independent variable there comes from a ratio of two measured quantities and hence the error is twice as large. There is another reason that is discussed briefly by Chung et al. [1988] which is that the more volatile part of the heavy oil (though small in quantity) evaporates during the experiment. It is expected that this evaporation would be less at higher pressures and indeed there is less scatter there. Mulliken and Sandler [1980] have also commented on this vaporization problem.

The tract that we have crossed in evaluating various transport and thermodynamic properties is a very large one. The fit to the available data are good and some predictive capabilities have been shown. It is worth emphasizing that we do not need the molecular weight of the crude oil anywhere. Here, the reference values of density and viscosity capture role played by molecular weights. This is not surprising. Reference densities for high density systems [Huang and O'Connell, 1987 and Brelvi and O'Connell, 1975] have been shown earlier to be sufficient in correlating thermodynamic properties. Similarly, the dependence of viscosity on molecular weight is well known in polymer melts [Berry and Fox, 1968]. Free volume theory used here has seen improvements. Sabbagh and Eu [2010], have provided both equilibrium and non-equilibrium statistical mechanics where

the oil can be imagined to be made of chains. The results are improvements to the free volume theory used here, except that the chain length, that is, the molecular weight of the oil, is needed. It is shown here, that the base case itself is sufficiently good to quantify the present system, and in any case the above improvements are difficult to apply. Purely empirical correspondence states results have been provided in an integrated form by Simon and Graue [1965] that are easy to use but lack depth.

The main question is if the parameters obtained for the oil used by Chung et al. [1988] can be transferred to other heavy oils. As mentioned earlier such possibility exists. If we scale the properties by the reference values to calculate the fractional changes (Eq.2.8, 2.10, 2.14, 2.1/2.26) then those changes are expected to be independent of the oil type. In fact Chung et al. [1988] have shown that the Welker and Dunlop [1963] relation (Eq.2.1 and 2.26) is satisfied by many heavy oils. However, more checking is needed.

3. A SINGLE PORE MODEL FOR DISPLACEMENT OF HEAVY CRUDE OIL WITH CO_2

3.1 INTRODUCTION

The present problem analyzes displacement of heavy crude oil in a capillary by CO_2 as seen in enhanced oil recovery. In immiscible displacement of viscous liquid in a tube by a gas with viscosity less than the liquid, a gas bubble moves steadily and leaves behind a thin liquid film of thickness h_∞ which is known as the Bretherton problem, an important problem in the area viscocapillary phenomena. With the recovery of crude oil in mind, the analysis has been confined to cylindrical pores ~ 1 μm and hence disjoining pressures are included and added to the Laplace pressures. We have focused on the region with the capillary numbers that are less than 0.01. We have provided the solutions to the mass transfer problem in the form of CO_2 dissolving in oil. It represents a first contribution to mass transfer in Bretherton problem in any form. In order to understand the mass transfer rate in form of dissolution of CO_2 in heavy crude oil under high pressure, we have included the changes of the physical properties of heavy crude oil on carbonation based on a real system. The thickness of thin oil films decreases with the presence of mass transfer which leads to an increase in oil recovery but decrease in carbonation. It is expected that the reverse is true at displacements at low capillary numbers where the disjoining pressure dominates. The numerical solutions have been obtained with FLUENT to obtain the results: profile shapes, capillary numbers, the thickness of thin oil films left behind and net mass transfer rates.

Crude oil is recovered from the petroleum oil fields first by mechanical means and then by flooding with brine. 67% of the original oil is still left behind. In addition,

these processes cannot be used in some oil fields that contain heavy oil. A key factor in brine flooding is the effect of brine-oil surface tension which gives rise to large retention of oil. One process that has been suggested to recover the remaining oil is CO_2 flooding. Some oil evaporates into the gas phase and some CO_2 dissolves in the oil, leading to miscibility [Hutchinson and Braun, 1961]. Miscibility cannot be attained in heavy oils but there too CO_2 flooding has some advantages. CO_2 swells the oil squeezing it from narrow pores and crevices and it reduces the viscosity of the heavy oil by up to a factor of 10, thus decreases the pressures needed to move the oil. Accepted boundary between light and heavy oils is a specific gravity of 0.9218 (API gravity of 22º) and viscosity of 0.1 Pa.s (100 cp) [USGS, 2003].

When a gas flows into a tube filled with a liquid, it does so in form of a finger [Bretherton, 1961]. Miller and Neogi [2008] considered other cases available in literature, a liquid displacing a gas and a liquid displacing another immiscible liquid, and summarized the results as shown in Figure 3.1. *A* is the displacing fluid (CO_2 here) and *B* is the displaced fluid (heavy oil). Figure 3.1 (a) is at equilibrium and the rock is assumed to be preferentially wet by *A*. As the velocity of displacement is increased, the equilibrium contact angle increases from zero in (a) to a dynamic contact angle of more than 90º (as measured through phase *A*) in (b) and finally to 180º in (c). At yet higher velocities entrainment takes place as shown in (d). A number of additional observations are:

(i) If the rock is preferentially wet by *B*, then the system starts from equilibrium at (b) and moves down to (c) and (d) on increasing the speed.

(ii) The viscosity ratio is $\chi = viscosity\ of\ A / viscosity\ of\ B$. If χ is near zero, the transition to (d) occurs at such low velocities that (a)-(c) are practically never observed. Conversely, if χ is very high, the transition occurs at very high velocities.

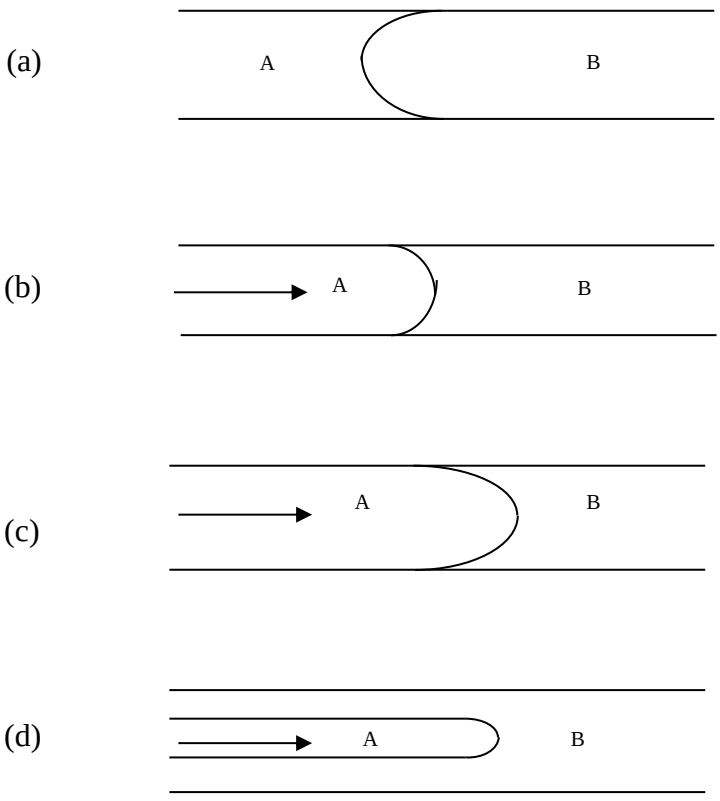

Figure 3.1. Fluid B is being displaced by fluid A. 3.1(a) shows equilibrium and that B is fully non-wetting. 3.1(b) and 3.1(c) show the dynamic contact angles α (measured through A) increases with increasing displacement velocity U. Finally in 3.1(d) the contact line has entrained.

The problem shown in Figure 3.1(d) is called the Bretherton [1961] problem who showed that the thickness of the film of *B* left behind was determined by hydrodynamics. If this thickness is h_∞,

$$h_\infty / R = 0.643(3Ca)^{2/3} \qquad (3.1)$$

where the capillary number $Ca = \mu U/\gamma$ where μ is the viscosity of liquid to be displaced and γ is the surface tension. U is the rate of movement of the gas bubble. Bretherton problem has remained a key problem in the area of viscocapillary flows. Bretherton however, worked with tubes of large radii. In the porous rock formation that contains the crude oil, the lower pore radii drops to ~ 0.1 μm and sometimes even lower. Here, the thin films will be greatly influenced by the disjoining pressure [Morrow, 1991] which is the negative of excess potential per unit volume due to the proximity of the walls. Teletzke et al. [1988] solved the Bretherton problem numerically where they included the disjoining pressures. They found that at very low displacement velocities, the effect of disjoining pressure dominates, but at larger velocities Bretherton's fluid mechanical results prevailed. Kreutzer et al [2005] have presented both experimental and theoretical results for movement at higher velocities. Giavedoni and Saita [1997] and Heil [2001] in their numerical solutions observe no difference in the profile shapes up to Ca = 5.0 and Reynolds numbers over 200.

One main difficulty lies in determining what ranges of capillary numbers to investigate. For enhanced oil recovery, Foster [1973] for instance indicates below 10^{-2} where 10^{-8} to 10^{-7} belongs to usually waterflooding. However, the viscosity of displacing fluid is used. Here, the fluid is CO_2 and its viscosity is about hundred times less than brine. Bretherton [1961] uses the viscosity of displacing oils which are more than a

thousand times less than the viscosity of heavy oils. We have kept capillary numbers below 10^{-2} for convenience.

We solve here the Bretherton's problem, with appropriate disjoining pressures for a CO_2- heavy oil system. However, the main feature that is considered is the effect of mass transfer and the accompanying changes in physical properties. Chung et al. [1988] have published detailed results for Bartlett crude, a heavy oil, with and without CO_2. Tran et al. [2012] have fitted these results to free volume theory. Only one temperature 297.1K (75ºF) is considered below. The list is

Henry's law constant H = 6.544x10^4 Pa(CO_2)/(kg/m^3)

Concentration of CO_2 in the oil at saturation in kg/m^3 $c_{sat} = p_{CO_2} / H$ and volume fraction $\phi_{sat} = 1.06x10^{-3} p_{CO_2} / H$.

Swelling factor $SF = \dfrac{1 - 5.917x10^{-5} p}{1 - \phi}$ where p is total pressure in atm.gage.

Density in g/cm^3 $\rho = \dfrac{\phi}{1.06} + \dfrac{0.94921}{SF}$ where $\phi = 1.06x10^{-3} c$ where c is the concentration in kg/m^3.

Viscosity in Pa.s $\ln \mu = \ln(14.8435) + [\dfrac{1}{f + \phi 4.5244x10^{-2}} - 47.89]$.

Free volume fraction without CO_2 is f = 0.02088 - 5.915x10^{-5}p.

Diffusivity in m^2/s $D = 5.14x10^{-13} e^{2.659c}$.

The surface tension Rojas and Ali [1988] is in mN/m where p_{CO2} is in MPa

$$\gamma = 24.626 + 0.4585 p_{CO_2} - 0.3652 p_{CO_2}{}^2$$

Consider Figure 3.2. If it is assumed that there is no flow in the liquid film left behind, then

$$\pi R^2 < v >= \pi (R - h_\infty)^2 U \tag{3.2}$$

where <*v*> is the average velocity far upstream from the nose of the bubble. In this region, the flow profile can be assumed to be the parabolic profile of Hagen-Poiseuille's flow.

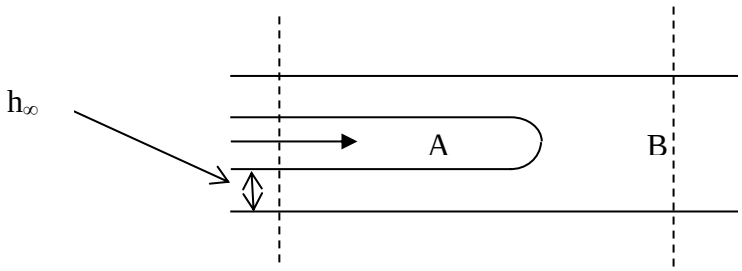

Figure 3.2. Using coordinates (say affixed to the nose of the meniscus), it is possible to say that for steady displacement, no dissolved CO_2 would have reached the station downstream, all of the liquid upstream would be saturated and if there is zero shear at the liquid-gas interface then the velocity in the liquid would be plug flow at U backwards.

In this problem it is assumed that CO_2 dissolves in the heavy oil that is being displaced, but no oil evaporates into the gas phase. To consider the overall rate of mass transfer, a moving coordinate system can be envisioned. CO_2 does not reach the station at the front, hence the only place CO_2 leaves the system is with the thin liquid film which can be considered to be saturated and velocity profile has a plug flow backwards at *U*. Hence the rate of mass transfer in mol/s

$$M = \pi \left[R^2 - (R - h_\infty)^2 \right] . U c_{sat} \tag{3.3}$$

where c_{sat} is the saturation concentration.

Experimental results on mass transfer have been reported for finite bubbles [Bercic and Pintar, 1997]. However, if it is assumed that the downstream liquid is saturated with CO_2 as in Eq. (3.3), a liquid side mass transfer coefficient cannot be calculated using their formulation. Numerical solution to the mass transfer problem for a finite bubble [van Baten and Krishna, 2011] also exists.

3.2 FORMULATION

The equations of motion, continuity and conservation of species (CO_2), as well as their boundary conditions (jump balances) are detailed elsewhere [Slattery, 1999]. These are solved to obtain, the velocity v, pressure p and concentration c. The fluids are considered to be compressible, the viscosity and diffusivity dependent on the local pressure and concentration of CO_2, and the surface tension at the CO_2-oil interface and solubility of CO_2 there, have been taken to depend on CO_2 pressure. The expressions for these functions have been given in the last section.

The problem is treated as an unsteady state problem where CO_2 is introduced at the entrance in a tube of $L/R = 20$, filled with heavy oil. However the oil viscosity is kept at 1.484 Pa.s, one order of magnitude lower than those for heavy oils, to help speed up the computation. The entrance region for the gas is determined using Eq. (3.1). After a period of rearrangement, the gas finger moves at a steady rate U into the tube originally filled with oil and leaving behind a lubricating layer of thickness h_∞. To keep the finger speed U steady, CO_2 is introduced at a constant volumetric flow rate at the entrance. U has to be measured separately by locating the nose tip of the finger ($z = z^*$) at different times and taking the slope. This slope is seen to be a constant. U is used to calculate the

capillary number *Ca*. The approach has a drawback that we cannot plan to come up at a predemetrmined value of capillary number. The pressure at the exit is set at zero. The pressure in the liquid falls linearly and the velocity profile there is parabolic indicating Hagen-Poiseuille flow. As expected there is practically no pressure drop in the gas phase but a vortex ring appears as shown in Figure 3.3

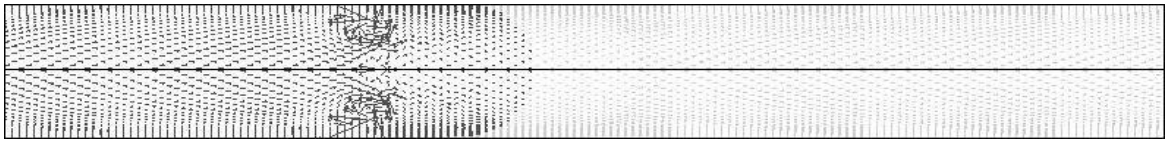

Figure 3.3. The vector diagram of the velocity field is shown. The vortex ring in the gas phase is easy to observe. Not so easy to observe is the parabolic velocity profile in the liquid, however it is revealed on closer inspection and the fact that the flow there is fully developed is easy to observe.

Thus, instead of using the pressure of CO_2 at the interface to calculate the surface tension and the solubility, the pressure at the entrance $p(0,0)$ that is, p at $z = 0$ and $r = 0$ is used, since the gas-liquid interface is not so easily located.

FLUENT is used to solve the problem using the volume of fluid (VOF) method [Wesseling, 2001]. Under discretization the shape of interface is no longer continuous nor can it be located exactly. There are two continuous variables of importance. The first is ϕ_g the volume fraction of the gas which is 1.0 in the CO_2 phase (A) and 0.0 in the oil phase (B). ϕ_g and other physical properties change continuously across the interface, which is no longer described as a singular surface. At the gaseous region of the inlet ϕ_g is set to 1.0. Another continuous variable is ψ, which is 0 in the CO_2 phase and 1 in the oil phase is actually used by the program instead of ϕ_g. Since ϕ_g changes continuously, the

interface is a wide band which can be made narrow by decreasing the size of the volume elements [Gupta et al. 2009]. As a result, whereas width of the elements in *z*-direction non-dimensionalized by *R* the tube radius, is kept at 0.1, the ones in *r/R* are progressively shortened. From the centerline the cell size moves outwards in 0.01 ninety nine times. The last section next to the wall is further divided hundred times to 0.0001 each. The reason for small volume elements in the *r*-direction next to the wall is that h_∞/R is a small number and smaller volume elements are needed to calculate this quantity accurately. Explicit scheme is used. FLUENT uses the method of Brackbill et al. [1992] to convert $2H\gamma$ to a body force. Whereas the code allows straightforward incorporation of the Laplace pressure, a separate program has to be used such that the disjoining pressure is incorporated as a body force using the same weight as for Laplace pressure. It is accounted for by augmenting Laplace pressure $2H\gamma$ to $2H\gamma + \Pi$ by writing a separate code with $h = R - r$ using in weight terms gradient of ψ described earlier, which drops to zeros in either bulk fluids.

Now, if we look at Figure 3.1, two types of interfaces are observed. From Figures 3.1(a) to 3.1(c), the interface is of finite extent but is of an infinite extent in 3.1(d). Teletzke et al. [1988] converted them all to interfaces of infinite extent by adding the disjoining pressure $\Pi(h)$. This needs to be included anyway as the deposited films have thicknesses in the range where disjoining pressure is important (< 0.1 μm). For profiles of finite extent, the thickness of the thin liquid film left behind is very small of the order of molecular thickness and below. Thus, these can be ignored, whence the interface becomes finite again. Teletzke et al. [1988] observed significant deviation from Eq. (3.1)

at small capillary numbers and very small tube dimensions. One model from Teletzke et al. [1988] for disjoining pressures is

$$\Pi = \frac{A_3}{h^3} - \frac{A_2}{h^2} \tag{3.4}$$

They used values of $A_3 = 10^{-21}$ J and $A_2 = 2\text{x}10^{-12}$ N. Deryaguin [1940]-Frumkin [1938] result for equilibrium contact angle λ for such a system is

$$\cos\lambda = 1 + \frac{2}{\gamma}\int_{h_o}^{\infty} \Pi dh \tag{3.5}$$

where h_o is the thickness of the thin film lying ahead of the bulk liquid at equilibrium. It follows that for $h_o = 4.985\text{x}10^{-10}$ m (4.985 Å), $\lambda = 33°$, where γ has been taken to be 25 mN/m. That is, the rock is not wet by oil. However, h_o has to be calculated as a part of the equilibrium profile. For A_2 equal to zero, oil will wet the rock. Hirasaki and Yang [1993] have provided additional information on the behavior of thin films in dynamic systems.

To obtain the concentrations of CO_2 in oil, we solve the conservation of species equation subject to the boundary condition that the concentration is c_{sat} at the gas-liquid interface. We override iterations for concentration in an element by setting it to zero for $\phi_g < 0.7$, or to c_{sat} for $0.4 < \phi_g < 0.7$, and allow the program to iterate when $\phi_g < 0.4$. The result that is sought is primarily h_∞, which as mentioned earlier, is where ϕ_g is closest to 0.5. The diffusivity has been set to $D(1\text{-}\phi_g)$.

3.3 RESULTS AND DISCUSSION

First, the results without mass transfer are considered. The shape of the profile for $Ca = 1.02 \times 10^{-4}$ is shown in Figure 3.4 at different times.

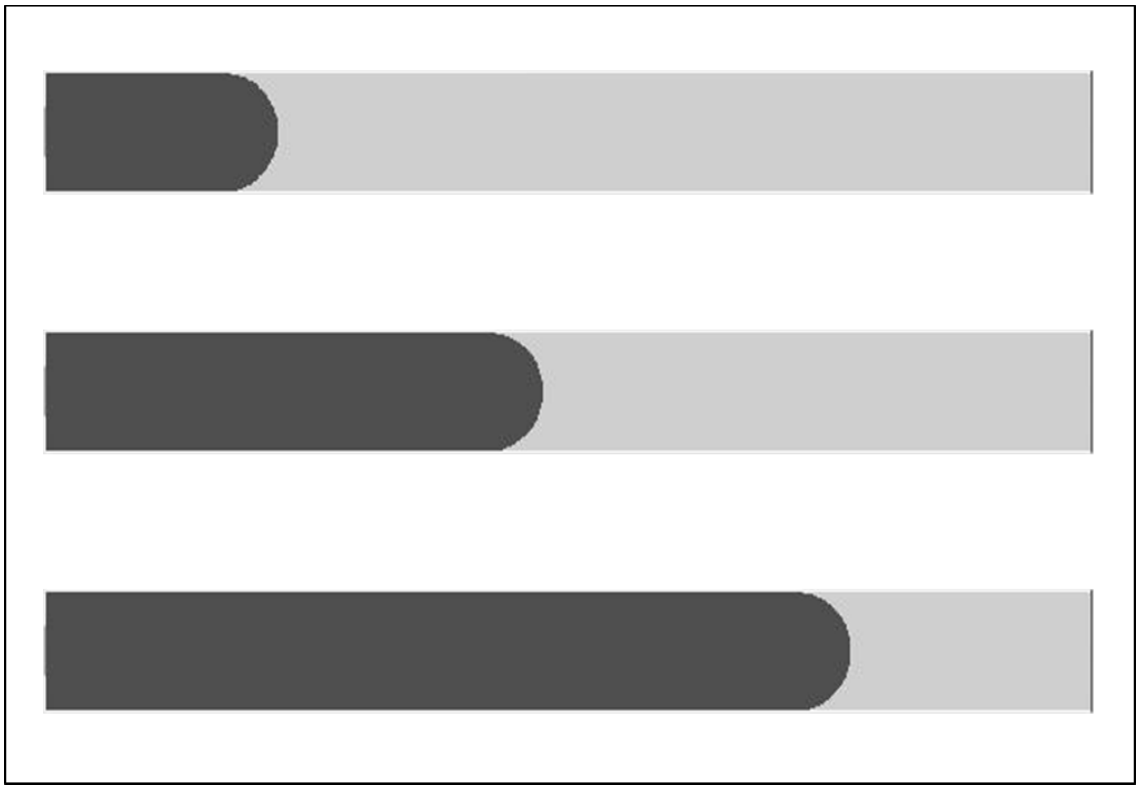

Figure 3.4. Profiles of the meniscus at $Ca = 1.02 \times 10^{-4}$ and R = 1 μm. The thickness of the deposited film h_∞ cannot be shown at this scale. The tip of the advancing meniscus is a spherical cap with a radius ≈ R.

The head is a spherical cap, a feature that does not change in all cases. At this scale h_∞ cannot be seen. The center-line pressure $p(z,0)$ has been shown in dimensionless

form in Figure 3.5 as a function of position z for the same capillary number at different times.

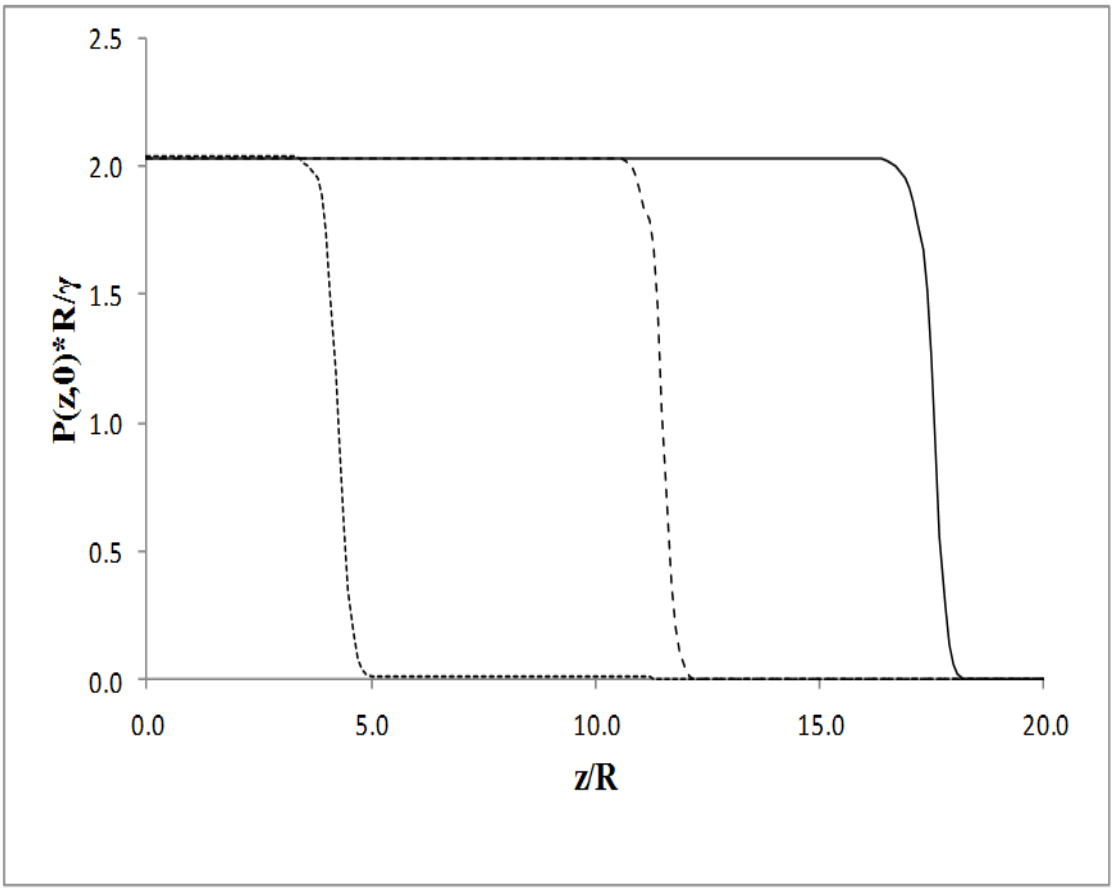

Figure 3.5. Dimensionless centerline pressure at $Ca = 1.02 \times 10^{-4}$ and R = 1 µm at different times.

Most of the pressure drop takes place across the interface. The Laplace pressure across the hemispherical cap is approximately $2\gamma/R$. Thus, if pressure is non-dimensionalized to $p(z,0)R/\gamma$, it should reach a value slightly in excess of 2. With this result in mind we have plotted the inlet pressure $p(0,0)$ in dimensionless form in Figure 3.6, for three different tube radii, all at a time where the menisci are at z^*/R in the tube

and capillary numbers are all comparable (but not equal). Since the pressure drop across the menisci, contribute to nearly all of the pressure drop, $p(0,0)$, the total pressure drop, is as expected ~ 2 in dimensionless form.

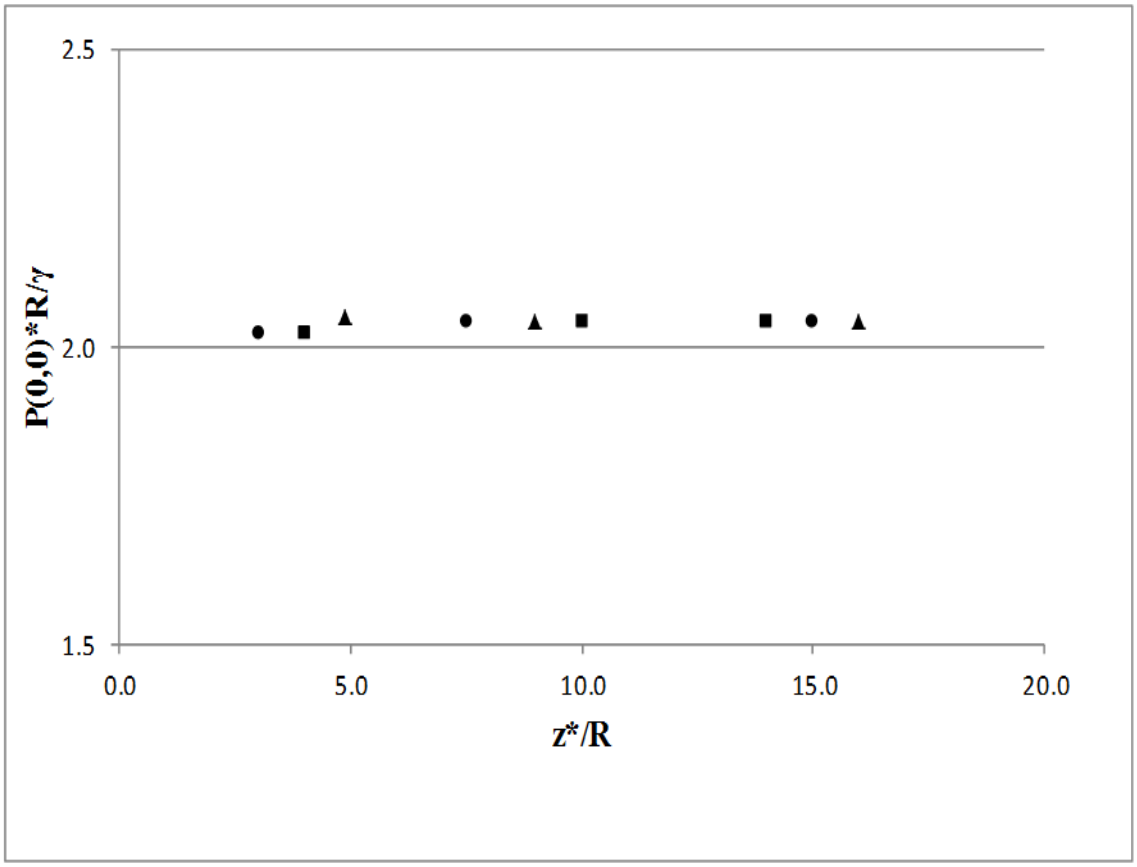

Figure 3.6. Dimensionless pressure at the origin at different times. z* gives the location of the nose of the bubble. The triangles give us Ca = 1.02×10^{-4} and R = 1 μm, the squares R = 10 μm and circles 0.1 μm. These last two cases have the same volumetric flowrate of CO_2 into the tube as the first case, but their capillary numbers differ somewhat.

In Figure 3.7, h_∞/R has been plotted against *Ca*. They are identical to Eq. (3.1) and the bubble shapes in those cases are same as those shown in Figure 3.4.

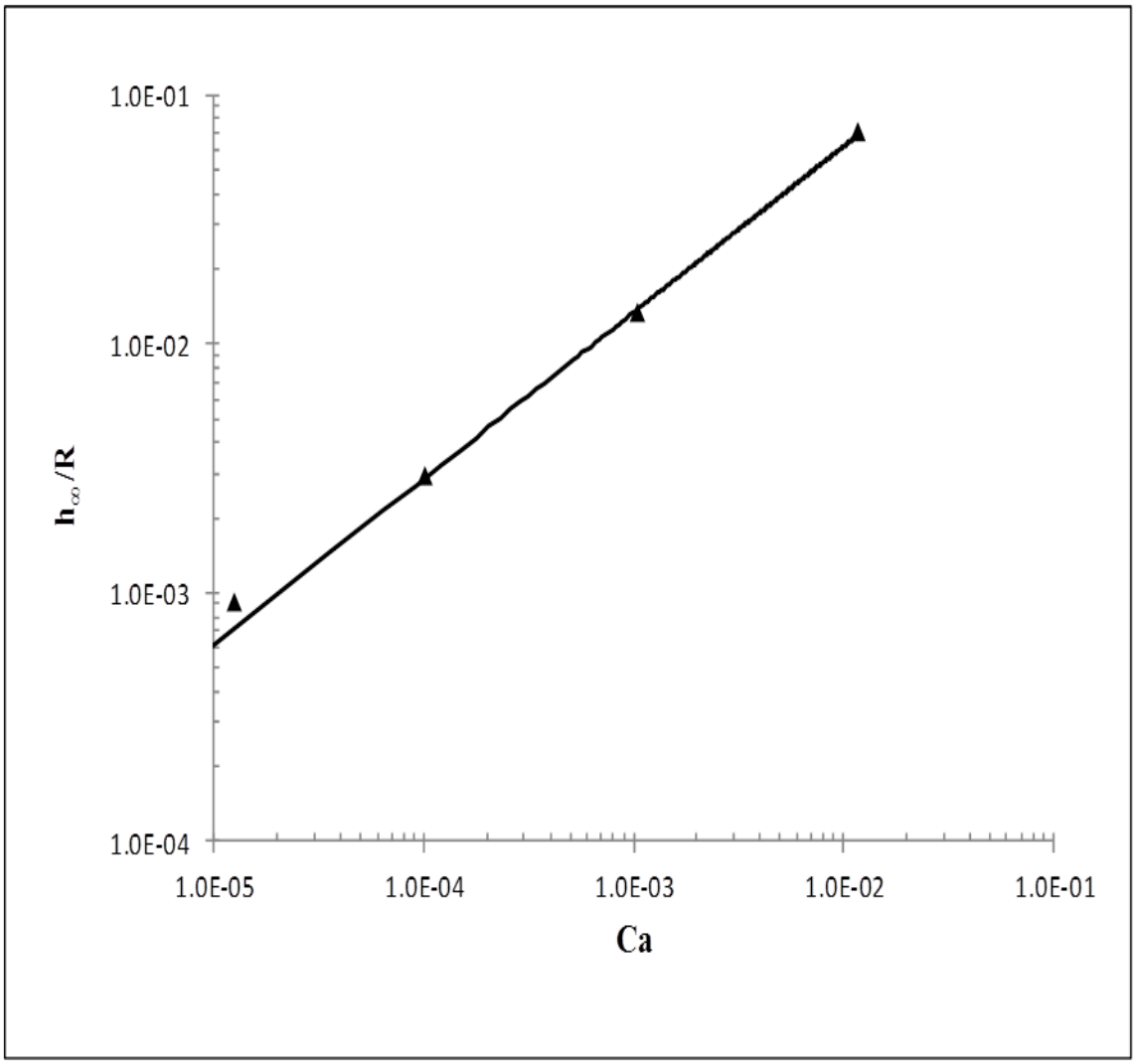

Figure 3.7. Bold line is the Bretherton result, Eq. (3.1) and the diamonds are results obtained numerically.

The disjoining pressures used are shown in Figure 3.8. When the disjoining pressure is in the form of Eq. (3.4) the film thickness is seen to be larger than that predicted by Bretherton, Eq. (3.1) in both cases as shown in Figure 3.9.

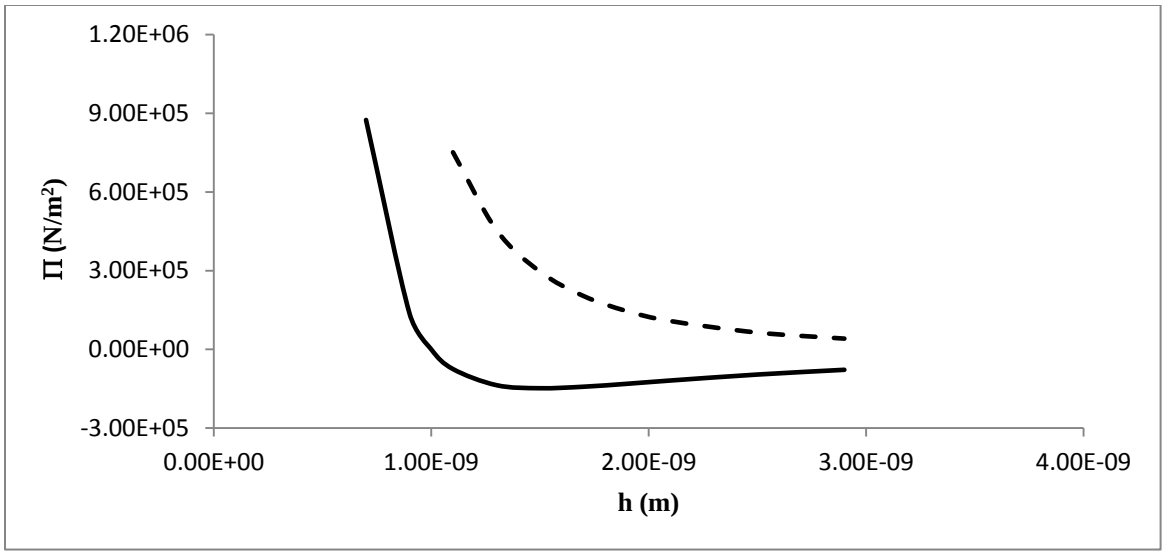

Figure 3.8. Disjoining pressure of Eq. (3.4) using constants that follow Eq.(3.4) have been plotted for a non-wetting (bold) and for a wetting (dashed) case. For the wetting case the second term on the right in Eq. (3.4) is deleted. For the non-wetting case, the region where dΠ/dh > 0 is unstable [Hirasaki, 1993].

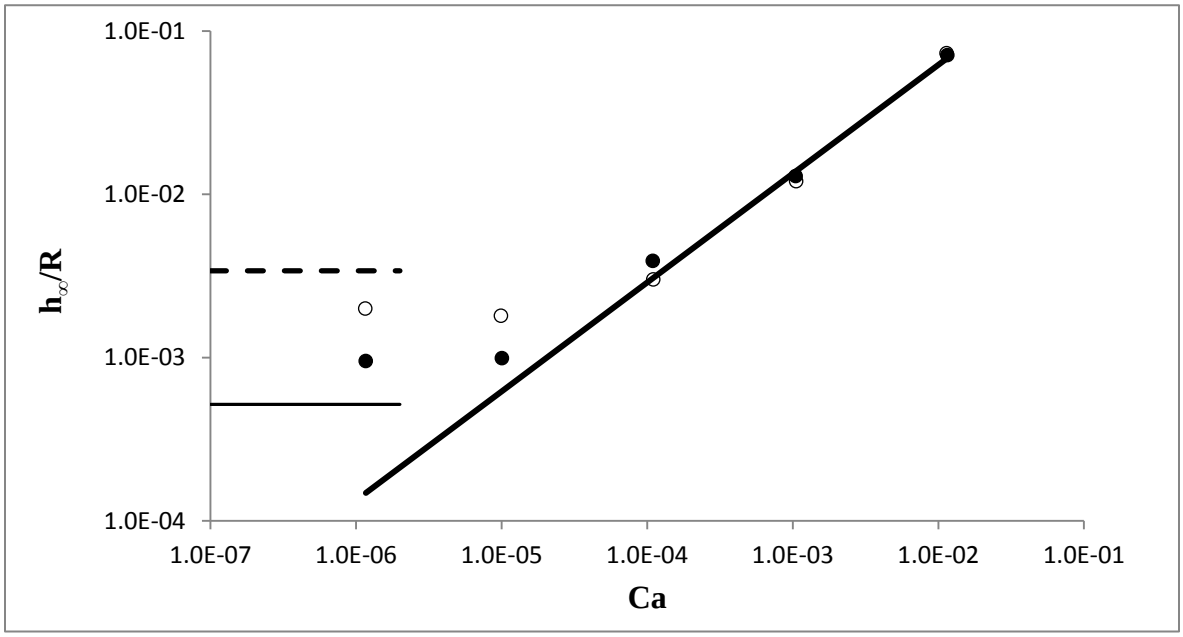

Figure 3.9. Film thicknesses are shown as a function of capillary numbers when disjoining pressures are included. The zero capillary number solutions from Eq. (3.6) have been plotted for the wetting (higher) and the non-wetting liquids using dashed lines. The results for the disjoining pressures for the wetting liquid are shown with white circles and those for the non-wetting liquids with black circles. Bretherton results, Eq. (3.1) have been shown in bold.

We know that to a good approximation that the pressure in the gas phase is $2\gamma/R$. However, the Laplace pressure in the thin film region is γ/R. Hence, the limiting thickness is the solution of

$$\frac{\gamma}{R} = \Pi \tag{3.6}$$

at very small capillary numbers, that is, negligible viscous effects. The solutions to Eq. (3.6) for the wetting and non-wetting liquids are shown with horizontal lines in Figure 3.9. The film thicknesses reach constant values when the capillary numbers are lowered but not the values predicted by Eq. (3.6) though they are close. The value is lower than that predicted by Eq. (3.6), 34.22 Å in case of wetting liquids. From their figures, Teletzke et al. [1988] see a lowered value as well (30 Å), although the deviation is small. For the non-wetting liquids, a larger thickness is seen in Figure 3.8 than 4.985Å predicted by Eq. (3.6). Teletzke et al. [1988] see no such signs of leveling off in the film thicknesses in the non-wetting case. The differences between the two cases, their's and our's, are mainly that the gas phase in the case studied by Teletzke et al. [1988] has been assumed to be inviscid but not here and that R in Eq. (3.6) is infinite (two parallel plates). For the non-wetting case, the film thicknesses from about 8Å to about 1000Å (the limit over which the effects of disjoining pressures are not felt) are all unstable [Dzyaloshinskii et al. 1960]. This covers most of the result for the non-wetting liquids. Film profiles are shown in Figure 3.10. For the non-wetting liquids the film thickness first makes a very low angle (almost zero), then as the film thins the slope increases (as appropriate for the receding case) to retain the equilibrium contact angle ~ 33^{o}. Thereafter the film has a constant thickness as envisaged in the Deryaguin-Frumkin equation, Eq. (3.5). For the

wetting liquid, the dynamic contact angle cannot fall below the equilibrium of 0^o as required for a receding case. So it retains 0^o throughout.

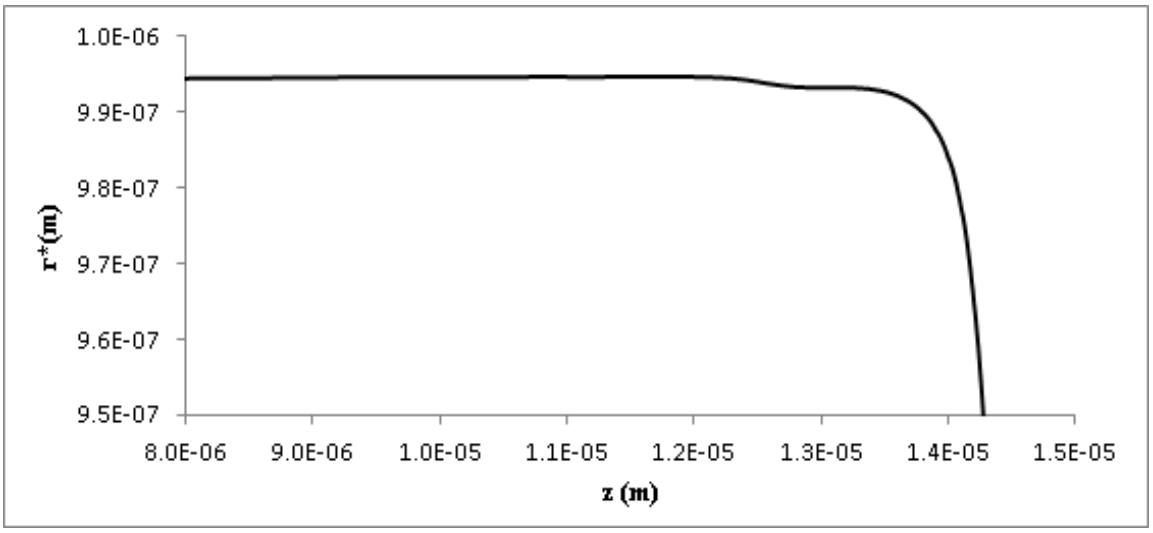

(a)

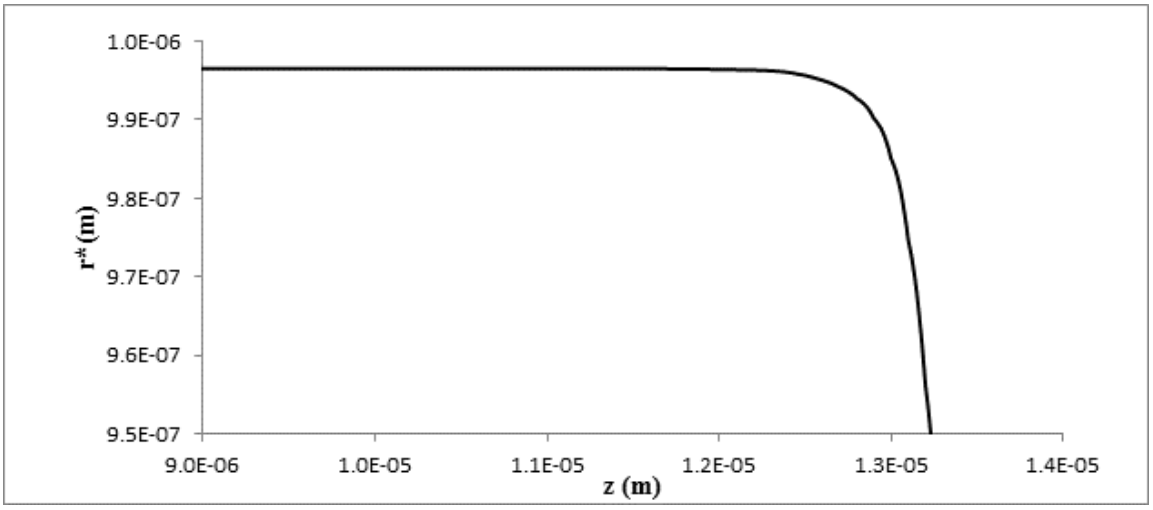

(b)

Figure 3.10. Film profiles have been shown for $Ca = 1.1037 \times 10^{-4}$, for the non-wetting (a) and wetting (b) cases. For the non-wetting case, the profile after it turns, is seen to change again to make the equilibrium contact angle.

From Eq. (3.3), it is possible to show that for small values of h_∞/R, the dimensionless mass transfer rate is to the first approximation, $2h_\infty/R$. Thus

$$\frac{M}{\pi R^2 c_{sat} U} = 1-(1-h_\infty / R)^2 \approx 2h_\infty / R \qquad (3.7)$$

The results of mass transfer calculations have been plotted in Figure 3.11 show that h_∞/R decreases some but the trend with the capillary number *Ca* remains about the same as predicted by Bretherton. In Figure 3.12, improvement in mass transfer has been plotted against the Peclet number $Pe = \frac{U 2R}{\bar{D}}$ where $\bar{D}$ is an average diffusivity, averaged from p_{sat} to zero.

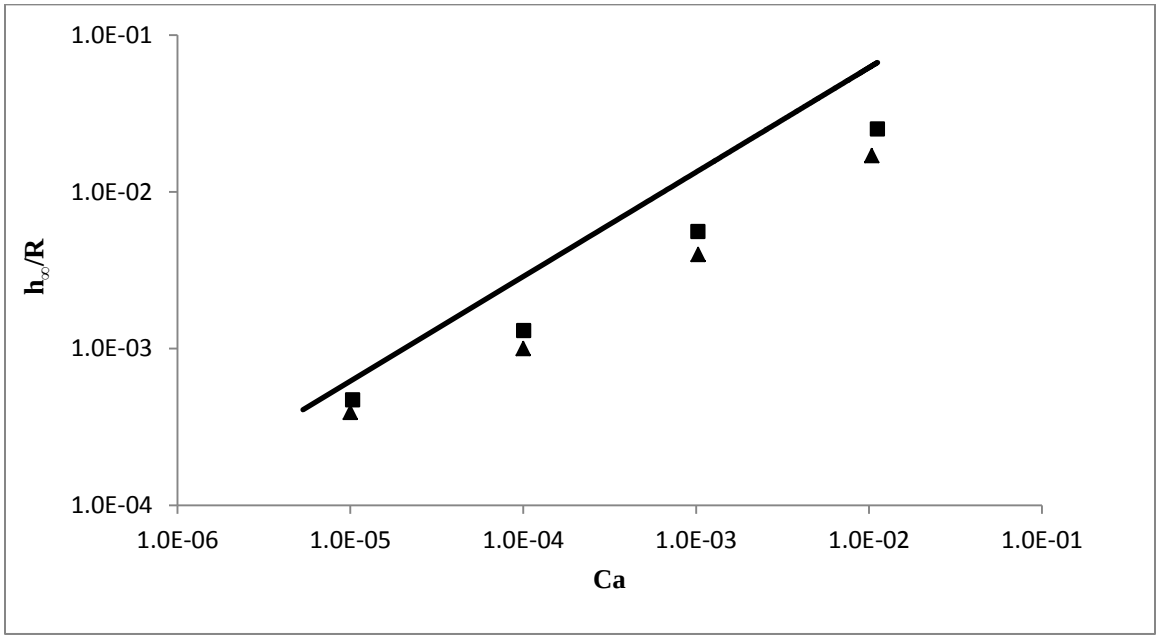

Figure 3.11. Effect of mass transfer without the inclusion of disjoining pressures is shown. The bold line is the Bretherton equation, Eq. (3.1). The black triangles are for tube radius of 1 μm and black squares are for 10 μm. Disjoining pressure has not been included.

It is observed in Figure 3.12 that with increasing convection, the mass transfer tends to reach a saturation where the improvement in mass transfer is plotted against *Pe*, quite contrary to intuition. The explanation for this negative impact of convection lies in the fact that in the front of the bubble, convection is in the direction opposite to the direction of diffusion. Now, increasing convection also squeezes the domain through which the CO_2 penetrates the oil at the tip of bubble. In fact, we were unable to draw the contour plots of CO_2 in oil in a meaningful way due to the very large compaction. However, the decrease in mass transferred is not without limits. More squeezing increases the concentration gradient and diffusive flux, reaching limits in a manner similar to concentration polarization.

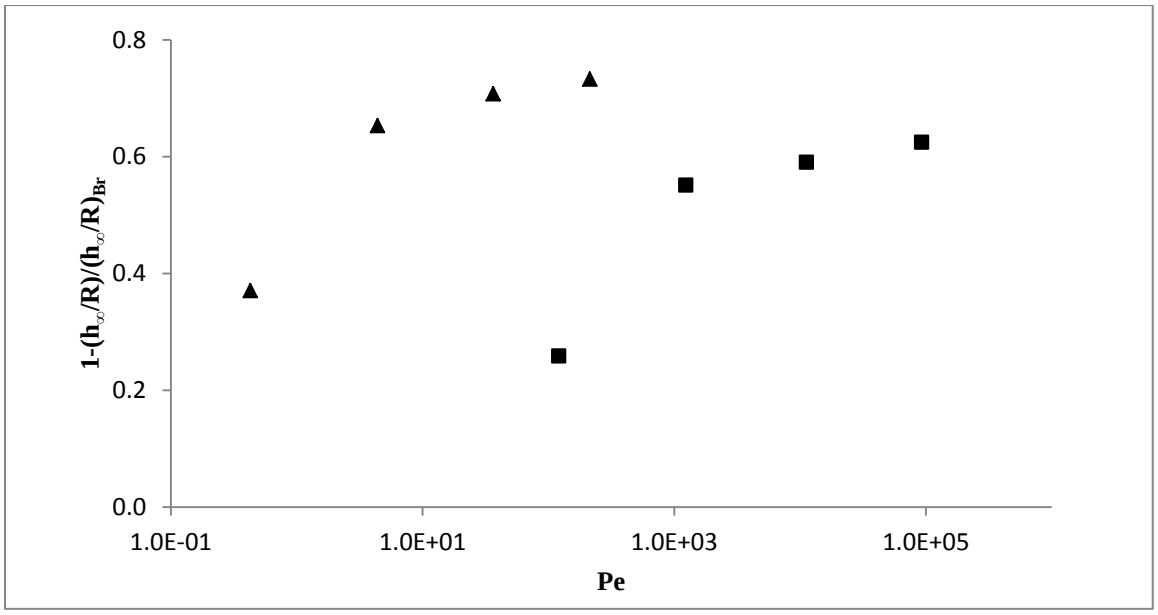

Figure 3.12. Mass transferred have been shown differently to illustrate that a saturation is reached. These have been plotted against Peclet numbers Pe that are proportional to tube diameter. Hence the great spread between the black triangles for tube radius of 1 μm and black squares for 10 μm. Disjoining pressure has not been included

In Figure 3.13 we have shown the decrease in capillary number due to mass transfer for the same inlet velocity and flow rate of the gas. This decrease takes place because a large volume of gas dissolves in the liquid at the interface. The countering effect of decrease in oil viscosity on carbonation is eventually not so significant. This decrease in velocity at the interface due to mass transfer is known to impart stability to a displacement process in oil recovery [Miller, 1975 and Tran et al. 2013].

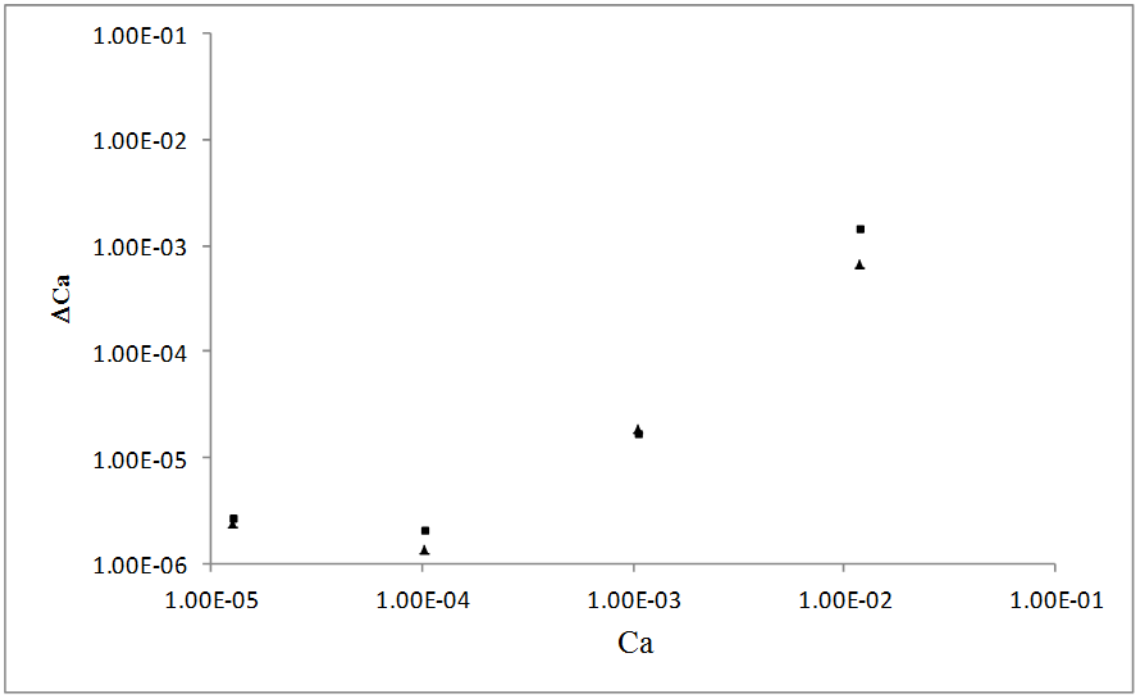

Figure 3.13. The decrease in capillary numbers Ca on including mass transfer as a function of Ca when the mass transfer is not included have been shown. The figure compares results obtained with and without mass transfer when the gas phase velocity and the flow rate at the entrance are equal.

None of the mass transfer results include the effects of disjoining pressures in the calculations but it is possible to say what those will be. As is evident in Figure 3.9, there is no effect at large capillary numbers. At small capillary numbers, Eq. (3.6) will still hold whether or not mass transfer is included. Hence thicker films and larger mass transferred will be observed, which are both known from the value of h_∞/R calculated from Eq. (3.6).

Finally, we look at some special features here. In Table 3.1, the effect of increasing the reference viscosity by an order of magnitude for one case has been shown. The gas pressure upstream ~ 1 atmg, that is, does not change significantly. The centerline pressure profiles remain about unchanged. With the same velocity and flow rate of the gas at the entrance, the velocity of the nose U remains practically unchanged. With the liquid viscosity up by an order of magnitude, the capillary number increases by an order. The decrease in h_∞/R on carbonation is higher for the oil with higher viscosity.

Table 3.1. Effect of oil viscosity for same inlet velocity of CO_2 in 1μm tube

	Reference viscosity 1.48 Pa.s	Reference viscosity 14.84 Pa.s
With no mass transfer	$Ca = 1.02 \times 10^{-4}$, $h_\infty/R = 2.90 \times 10^{-3}$	$Ca = 1.07 \times 10^{-3}$, $h_\infty/R = 1.30 \times 10^{-2}$
With mass transfer	$Ca = 1.00 \times 10^{-4}$, $h_\infty/R = 1.00 \times 10^{-3}$	$Ca = 1.05 \times 10^{-3}$, $h_\infty/R = 4.67 \times 10^{-3}$

4. STABILITY OF CO_2 DISPLACEMENT OF AN IMMISCIBLE HEAVY OIL IN A RESERVOIR

4.1 INTRODUCTION

Carbon dioxide (CO_2) flooding was originally viewed as a process where some CO_2 would dissolve in the crude oil and some oil would evaporate leading to miscibility [Hutchinson and Braun, 1961]. When that happens, the adverse effects of oil-gas interfacial tension disappear and a much lower amount of oil is left behind in a drive. The problem of unfavorable mobility ratio remains [Neogi, 1987; Saffman and Taylor, 1958; Chuoke et al. 1959; Scheidegger, 1960; Outmans, 1962; Rachford, 1964; Perkin and Johnston, 1969; Hagoort, 1974; Craig, 1971] which gives rise to poor sweep efficiencies. Heavy oils are not miscible, nevertheless even for heavy oils, CO_2 flooding can be a good candidate because when it dissolves in oil, the oil viscosity drops by 90% [Chung et al. 1988]. It has also been shown that on dissolution of CO_2 in oil, the oil swells [Chung et al. 1988; Welker and Dunlop, 1963] and it is suggested that this would help the oil to come out of narrow capillaries and lower the retention. However, the stability problem remains and only CO_2 with foam thickeners appear to be recommended [Smith, 1988]. Success in CO_2 flooding of oil fields with heavy oils has been reported [Issever and Pamir, 1993; Paracello, 2012; Kang et al. 2013]. Gravity assisted drainage schemes are also being suggested to overcome the stability problem. On the other side is the problem of CO_2 sequestration [Bachu and Shaw, 2003; Shaw and Bachu, 2002] in a heavy oil reservoir. The CO_2 can move out of the well by carbonation and actual displacement of carbonated oil. If the speed of displacement is significant one has enhanced oil recovery, and if it is insignificant then we only have sequestration. In both

cases, one has a CO_2-oil interface and the issue of stability arises. The key problem of how to displace heavy oil itself is not being considered, its stability is.

Below, we have analyzed the displacement process in an idealized reservoir. The solution is used next in a linear stability analysis. Very surprisingly, the result shows that the front is mainly stable, in spite of an exceedingly large adverse mobility ratio. The quantitative information could be obtained only because of the physical properties correlated earlier [Tran et al. 2012] based on experimental data [Chung et al. 1988] on heavy crude.

4.2 BASE CASE

The displacement system is shown in Figure 4.1. It is assumed that the oil can be represented as a single pseudo component and vaporizes into CO_2 phase, just as CO_2 dissolves into the oil. However, miscibility is not reached.

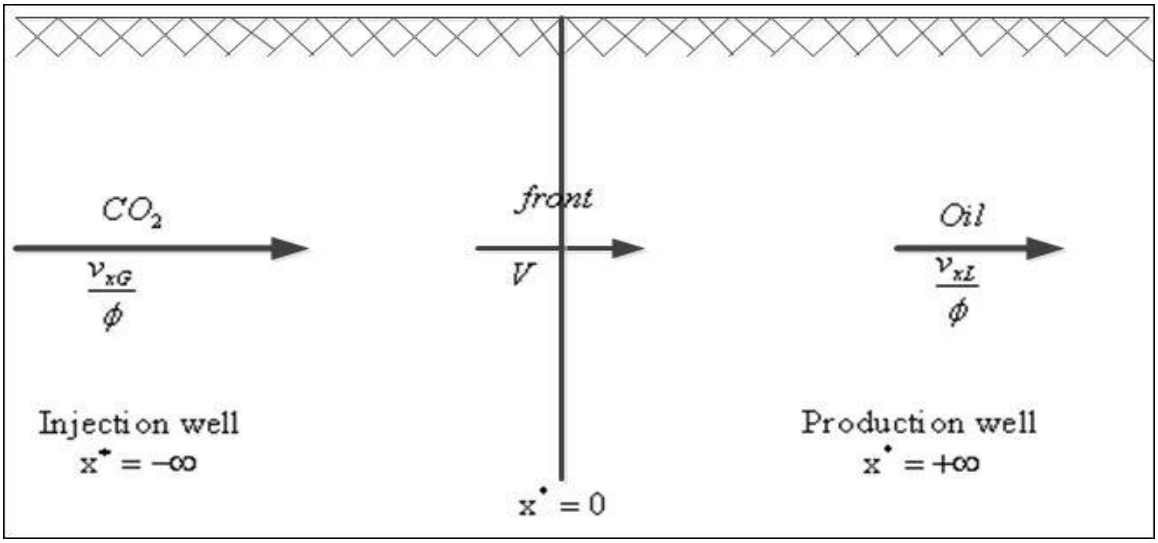

Figure 4.1. Schematic view of the flooding process and the basic setup for the formulation are shown. The arrows are approximately proportional to the velocities.

The continuity equations in the two phases, *G* the gas phase and *L* the oil phase, are

$$\frac{\partial \rho_G}{\partial t} + \frac{\partial}{\partial x}\left(\frac{v_{xG}}{\phi}\rho_G\right) = 0 \tag{4.1}$$

$$\frac{\partial \rho_L}{\partial t} + \frac{\partial}{\partial x}\left(\frac{v_{xL}}{\phi}\rho_L\right) = 0 \tag{4.2}$$

where x is the direction of flow, t is the time and ρ is the density. The velocities v_{xi} are governed by Darcy's law.

$$v_{xG} = -\frac{k_G}{\mu_G}\frac{\partial P_G}{\partial x}; v_{xL} = -\frac{k_L}{\mu_L}\frac{\partial P_L}{\partial x} \tag{4.3}$$

where k_G and k_L are the effective permeabilities in the two phases taken to be constants.

The displacement is assumed to be complete. It is assumed that the volumes are additive, hence ρ s are constants, leading to v_{xG} and v_{xL} the superficial velocities, to be constants. The jump mass at the interface is

$$\rho_G\left(\frac{v_{xG}}{\phi} - V\right) = \rho_L\left(\frac{v_{xL}}{\phi} - V\right) = c \tag{4.4}$$

where V is the velocity of the front and c is the net mass transferred across the interface, both are functions of time. The oil has been assumed to be displaced completely. The conservation equations for the two species are

$$\frac{\partial C_{Gi}}{\partial t} + \frac{v_{xG}}{\phi}\frac{\partial C_{Gi}}{\partial x} = D_{G\ell}\frac{\partial^2 C_{Gi}}{\partial x^2} \tag{4.5}$$

$$\frac{\partial C_{Li}}{\partial t} + \frac{v_{xL}}{\phi}\frac{\partial C_{Li}}{\partial x} = D_{L\ell}\frac{\partial^2 C_{Li}}{\partial x^2} \tag{4.6}$$

where the component i = 1 is for CO_2 and 2 is for oil. $D_{G\ell}$ and $D_{L\ell}$ are the longitudinal dispersion coefficients in the two phases assumed to be the same for either component. The solutions are

$$C_{Gi} = A_{Gi} + B_{Gi} erf[\frac{x - v_{xG} t/\phi}{\sqrt{4D_{G\ell} t}}] \tag{4.7}$$

$$C_{Li} = A_{Li} + B_{Li} erf[\frac{x - v_{xL} t/\phi}{\sqrt{4D_{L\ell} t}}] \tag{4.8}$$

where the As and Bs are constants. The boundary conditions are determined by concentrating on the interface at $x = L$, in which case the injection well is far upstream at $x = -\infty$ and production well is far downstream at $x = +\infty$. Hence,

$$C_{Gi} = C_{Gi}^0 \ at \ x = -\infty \quad \text{(injection conditions)} \tag{4.9}$$

$$C_{Li} = C_{Li}^o \ at \ x = +\infty \quad \text{(production)} \tag{4.10}$$

$$C_{Gi} = m_i C_{Li} \ at \ x = L \quad \text{(front)} \tag{4.11}$$

where m_i are the partition coefficients. The species balances at the interface lead to

$$(\frac{v_{xG}}{\phi} - V) C_{Gi} - D_{Gi} \frac{\partial C_{Gi}}{\partial x} = (\frac{v_{xL}}{\phi} - V) C_{Li} - D_{Li} \frac{\partial C_{Li}}{\partial x} = d_i \quad x = L \tag{4.12}$$

where d_i is the amount of species i transferred across the interface.

The pressures in the two phases P_G and P_L differ at the front by the capillary pressures. Due to the approximations used earlier, the normal stress balance at the front is not required. Nevertheless we have used two different symbols to denote that the two pressures are not equal anywhere.

An assumption is made that

$$c = \frac{\chi}{\sqrt{t}} \tag{4.13}$$

leading to

$$V = \frac{v_{xG}}{\phi} - \frac{\chi}{\rho_G \sqrt{t}} = \frac{v_{xL}}{\phi} - \frac{\chi}{\rho_L \sqrt{t}}$$

Now, $L = \int_0^t V dt$, hence

$$L = \frac{v_{xG}}{\phi} t - \frac{2\chi}{\rho_G} \sqrt{t} = \frac{v_{xL}}{\phi} t - \frac{2\chi}{\rho_L} \sqrt{t} \qquad (4.14)$$

In addition

$$d_i = \frac{\chi_i}{\sqrt{t}} \qquad (4.15)$$

$$\chi = \chi_1 + \chi_2 \qquad (4.16)$$

These equations and boundary conditions are enough to determine the constants *A*s, *B*s and χs. However, it is necessary to be consistent with constant density conditions and the conditions at the wells, leading to the requirements that $C_{G1}^o = \rho_G; C_{G2}^o = 0$ and $C_{L1}^o = 0; C_{L2}^o = \rho_L$ where the densities are those taken at the interface.

Following Hutchinson and Braun [1961] we have taken heavy oil to be C_{10}. From Reamer and Sage [1963] estimates for the CO_2-C_{10} system are found to be ρ_L = 7.51173x10^{-3} mol/cm^3, ρ_G = 1.06383x10^{-3} mol/cm^3, m_1 = 0.4536 and m_2 = 0.000023 over reasonable temperatures and pressures (~ 29°C and 2MPa). It is evident that m_2 can be taken to be zero. This means that C_{10}, in our model for heavy oil, is practically nonvolatile. For this approximation, $\chi_1 = \chi$ and $\chi_2 = 0$. The boundary conditions lead to

$$\chi\left(1 - \frac{\rho_G}{\rho_L m_1}\right) erfc\left(\frac{\chi}{\rho_L \sqrt{D_{L\ell}}}\right) - \frac{\rho_G}{m_1} \sqrt{\frac{D_{L\ell}}{\pi}} e^{-\frac{\chi^2}{\rho_L \sqrt{D_{L\ell}}}} = 0 \qquad (4.17)$$

where $D_{L\ell}$ and in the present case is approximately the molecular diffusivity [Lake, 1988; Hewett et al. 1988] which is about 10^{-5} cm^2/s. For the values of the physical properties given, $\chi = 3.81525 \times 10^{-5}$ mol/ ($cm^2.s^{1/2}$).

In view of these results, we note that it is also possible to use the correlation for the solubility [Tran et al. 2012] of CO_2 in heavy oil from the data by Chung et al. [1988] which presupposes that the oil is non-volatile. Their value for m_1 is ~ 1.15 ignoring complications in CO_2 phase behavior at pressures much higher than 2 MPa used above. It is noteworthy that Tran et al. [2012] showed Henry's law to remain valid up 2000 psi. If m_1 increases to infinity, Eq. (4.11) shows that the solubility of CO_2 in oil drops to zero. We also distinguish between m_1 and the value of C_{L1} at the interface. Only the value of C_{L1} and not m_1 that is needed to evaluate the stability results obtained below. In Eq. (4.11) it is the gas phase concentration of CO_2 that can be independently varied by changing the pressure and hence C_{L1} can be increased by increasing the gas pressure even when m_1 is small.

4.3 STABILITY

In the stability analysis of the system we provide perturbations to all quantities which are related to one another through conservation equations and boundary conditions. The base case varies in space and time, but it is assumed that the disturbances change more rapidly such that in the analysis they are assumed to be constants. The emphasis here is on the mass transferred between phases and the lowering of oil density and viscosity by CO_2. Darcy's law with continuity leads to

$$\frac{\partial^2 P_i}{\partial x^2} + \frac{\partial^2 P_i}{\partial y^2} + \frac{\partial^2 P_i}{\partial z^2} = 0 \tag{4.18}$$

Now

$$P_i = \overline{P}_i + P_i' \tag{4.19}$$

where overbars represent the base case results of the earlier section and primes indicate disturbances which are functions of position and time. By substituting Eq. (4.19) into Eq. (4.18) and using the base case we have

$$\nabla^2 P_i' = 0 \tag{4.20}$$

This equation is valid for the gas phase only, $i = G$. The solution is sought in the form of a Fourier component

$$P_G' = \pi_G(x) f(y,z) e^{\beta t} \tag{4.21}$$

where

$$\left[\frac{d^2}{dy^2} + \frac{d^2}{dz^2}\right] f = -\alpha^2 f \tag{4.22}$$

and α is wave number = 2π / wave length of the disturbances leading to

$$\frac{d^2 \pi_G}{dx^2} - \alpha^2 \pi_G = 0 \tag{4.23}$$

$$\pi_G = A_1 e^{\alpha(x-\bar{L})} \tag{4.24}$$

where subsequently we will use as independent variable $x^* = x - \bar{L}$. All disturbances decay far from the interface, $x^* = 0$. In the liquid phase

$$v_{xL}' = -\frac{k_L}{\bar{\mu}_L}\frac{\partial P_L'}{\partial x^*} + \frac{k_L}{\bar{\mu}_L^2}\frac{\partial \bar{\mu}_L}{\partial \bar{C}_{L1}} C_{L1}' \frac{\partial \bar{P}_L}{\partial x^*} \tag{4.25}$$

On linearization leading to

$$\nabla^2 P_L' = \frac{\partial \ln \bar{\mu}_L}{\partial \bar{C}_{L1}} \cdot \frac{\partial \bar{P}_L}{\partial x^*} \frac{\partial C_{L1}'}{\partial x^*} \tag{4.26}$$

where Darcy's law has been used and then a divergence is taken. An effort to preserve the concentration dependence of the liquid viscosity has been also made. We take

$$P_L' = \pi_L(x^*) f(y,z) e^{\beta t} \tag{4.27}$$

We also look at the concentration fluctuations

$$C_{ij}' = \xi_{ij}(x^*) f(y,z) e^{\beta t} \tag{4.28}$$

It results in

$$D_{i\ell} \frac{d^2 \xi_{ij}}{dx^{*2}} - (\frac{\bar{v}_{xG}}{\phi} - V) \frac{d\xi_{ij}}{dx^*} - (\beta + D_{it}\alpha^2)\xi_{ij} = \frac{\partial \bar{C}_{L1}}{\partial x^*} (-\frac{k}{\phi \bar{\mu}_L} \frac{d\pi_L}{dx^*} - \frac{\bar{v}_{xL}}{\phi} \frac{\partial \ln \bar{\mu}_L}{\partial \bar{C}_{L1}} \xi_{L1} - \beta a) \tag{4.29}$$

where besides the longitudinal dispersion, the transverse dispersion has also been included where the dispersivities are taken to be the same for both species. The right hand side exists only when $i = L$ and $j = 1$. The boundary changes from $x^* = 0$ to $x^{*\prime} = a.f.e^{\beta t}$ where a is a constant. Darcy's law has been used. Eq. (4.26) becomes

$$\frac{d^2}{dx^{*2}} \pi_L - \alpha^2 \pi_L = \frac{\partial \ln \bar{\mu}_L}{\partial \bar{C}_{L1}} \cdot \frac{\partial \bar{P}_L}{\partial x^*} \frac{\partial \xi_{L1}}{\partial x^*} \tag{4.30}$$

Eqs. (4.29) and (4.30) can be solved but the solutions that result are very complicated and some simplification is sought below. The intermediate steps so far have been supplied for the pressures only.

The solutions to Eq. (4.29) subject to the condition that disturbances disappear far from the interface are

$$\xi_{G1} = A_3 e^{\gamma_1 x^*} \; ; \; \xi_{G2} = A_4 e^{\gamma_1 x^*} \tag{4.31}$$

and

$$\xi_{L2} = A_6 e^{\gamma_2 x^*} \tag{4.32}$$

where

$$\gamma_1 = \frac{(\frac{\bar{v}_{xi}}{\phi} - V) + \sqrt{(\frac{\bar{v}_{xi}}{\phi} - V)^2 + 4D_{i\ell}(\beta + D_{it}\alpha^2)}}{2D_{it}} > 0 \tag{4.33a}$$

$$\gamma_2 = \frac{(\frac{\bar{v}_{xi}}{\phi} - V) - \sqrt{(\frac{\bar{v}_{xi}}{\phi} - V)^2 + 4D_{i\ell}(\beta + D_{it}\alpha^2)}}{2D_{it}} < 0 \tag{4.33b}$$

where the difference between the two velocities for $i = G$ and L are given in Eq. (4.4). The signs on γ are sufficient to make the disturbances vanish in their phases. The case of $i = L$ and $j = 2$, that is, CO_2 in the oil phase is more difficult to solve. We make an assumption to simplify matters in that we take the effect of pressure fluctuation in the liquid phase to have a negligible effect on the concentration fluctuations, that is, the first term on the right hand side in Eq. (4.29) is neglected. The reason is that there are two terms describing convective effect. Of these, the one ignored appears to be attenuated by an additional factor $\frac{\partial \bar{C}_{L1}}{\partial x^*}$. The result is

$$\xi_{L1} = A_5 e^{\gamma_3 x^*} + \frac{\beta a}{(\beta + D_{Lt}\alpha^2)} \frac{\partial \bar{C}_{L1}}{\partial x^*} \tag{4.34}$$

$$\gamma_3 = \frac{\Delta V - \sqrt{\Delta V^2 + 4D_{L\ell}(\beta + D_{Lt}\alpha^2)}}{2D_{L\ell}} < 0 \tag{4.35}$$

where $\Delta V = \frac{\bar{v}_{xL}}{\phi} - V - \bar{v}_{xL} \frac{\partial \ln \bar{\mu}_L}{\partial \bar{C}_{L1}} \frac{\partial \bar{C}_{L1}}{\partial x^*}$. Further,

$$\pi_L = A_2 e^{-\alpha x^*} + a_1 e^{\gamma_3 x^*} \tag{4.36}$$

where $a_1 = \frac{\Lambda_1 A_5 \gamma_3}{\gamma_3^2 - \alpha^2}$, $\Lambda_1 = -\frac{\bar{v}_{xL}}{k_L}\frac{\partial \bar{\mu}_L}{\partial \bar{C}_{L1}}$ and Darcy's law has been used.

It is now necessary to apply the solutions to the boundary conditions at $x^{*\prime}$ which are now referred back to $x^* = 0$. The pressure balance at the interface in terms at $x^* = 0$ leads to

$$A_2 + \frac{\Lambda_1 A_5 \gamma_3}{\gamma_3^2 - \alpha^2} - \rho_L g_x a - \frac{\bar{\mu}_L}{k_L}\bar{v}_{xL} a = A_1 - \rho_G g_x a - \frac{\bar{\mu}_G}{k_G}\bar{v}_{xG} a \tag{4.37}$$

So far we have been using dynamic pressures for analysis but the above balance is on the static pressures. Hence, gravity has been subtracted and g_x is the component of gravity in the x-direction. The partitioning at the interface leads to

$$A_3 = m_1 A_5 + m_1 \frac{\partial \bar{C}_{L1}}{\partial x^*} a \tag{4.38}$$

and to $A_4 = 0$. Further, we have been assuming throughout that the density of each phase is a constant. In the gas phase it leads to $\xi_{1G} + \xi_{2G} = 0$ or $A_3 + A_4 = 0$. As A_4 is zero since there is no oil in the gas phase, $A_3 = 0$. However, it is not possible to apply a constant density condition overall in the liquid phase, but can be applied at $x^* = 0$. It leads to

$$A_5 + \frac{a\beta}{\beta + D_{Lt}\alpha^2}\frac{\partial \bar{C}_{L1}}{\partial x^*} + A_6 = 0 \tag{4.39}$$

where these terms represent the sum of ξ_{1L} and ξ_{2L}, and A_6 is the constant in ξ_{2L}. At $x^* = 0$ the perturbation to Eq. (4.4), leads to

$$\rho_G\left(\frac{k_G}{\phi\mu_G}\alpha A_1 + a\beta\right) = \rho_L\left(\frac{k_L}{\phi\mu_L}(-\alpha A_2 + a_1\gamma_3) + \frac{\bar{v}_{xL}}{\phi}\frac{\partial \ln \bar{\mu}_L}{\partial \bar{C}_{L1}}\left(A_5 + \frac{a\beta}{\beta + D_T\alpha^2}\frac{\partial \bar{C}_{L1}}{\partial x^*}\right) + a\beta\right) \tag{4.40}$$

The last boundary condition, the perturbation to Eq. (4.5) for the balance of fluxes of species 1, is given by

$$-a\beta\bar{C}_{1G} = -\bar{C}_{1L}\left(\frac{k}{\phi\mu_L}(-\alpha A_2 + a_1\gamma_3) + \frac{\bar{v}_{xL}}{\phi}\frac{\partial \ln \bar{\mu}_L}{\partial \bar{C}_{L1}}\left(A_5 + \frac{a\beta}{\beta + D_{Lt}\alpha^2}\frac{\partial \bar{C}_{L1}}{\partial x^*}\right) + a\beta\right)$$
$$+\left(A_5 + \frac{a\beta}{\beta + D_{Lt}\alpha^2}\frac{\partial \bar{C}_{L1}}{\partial x^*}\right)\left(\frac{\bar{v}_{xL}}{\phi} - \bar{V}\right) - D_{L\ell}A_5\gamma_3 \tag{4.41}$$

4.4 RESULTS AND DISCUSSION

It is now possible to combine Eqs. (4.37- 4.41) to write a matrix equation in the form of

$$\underline{\underline{Q}}\,\underline{A} = \underline{0}, \tag{4.42}$$

where $\underline{\underline{Q}}$ is a 5x5 matrix and $\underline{A}$ is a column vector consisting of the unknowns A_1, A_2, A_5, A_6, a. For this set of homogeneous equations to yield a non-trivial solution, the determinant of $\underline{\underline{Q}}$ must vanish which gives us the dispersion equation in the form of β as a function of wavenumber α. We look at the case of marginal stability where $\beta = 0$.

It leads to

$$(\rho_G - \rho_L)g_x + \left(\frac{\bar{\mu}_L}{k_L}\bar{v}_{xL} - \frac{\bar{\mu}_G}{k_G}\bar{v}_{xG}\right) + \frac{\left(-\frac{\partial \bar{C}_{L1}}{\partial x^*}\right)[(q_{32}+q_{31})q_{53} - (q_{33}+q_{31}q_{23})q_{52}]}{q_{52}q_{31}} = 0 \tag{4.43}$$

where q_{ij}s are elements of $\underline{\underline{Q}}$. The ones that we need are

$$q_{23} = \frac{\Lambda_1\gamma_3}{\gamma_3^2 - \alpha^2}, \quad q_{31} = \frac{\rho_G k_G \alpha}{\phi\mu_G}, \quad q_{32} = \frac{\rho_L k_L \alpha}{\phi\mu_L}, \quad q_{33} = -\left[\frac{\rho_L k_L \Lambda_1 \gamma_3}{\phi\mu_L(\gamma_3^2 - \alpha^2)} + \frac{\rho_L \bar{v}_{xL}}{\phi}\frac{\partial \ln \bar{\mu}_L}{\partial \bar{C}_{L1}}\right],$$

$$q_{52} = \frac{\bar{C}_{1L}k_L\alpha}{\phi\mu_L},$$

$$q_{53} = \left[\frac{\bar{C}_{1L} k_L \Lambda_1 \gamma_3^2}{\phi \mu_L (\gamma_3^2 - \alpha^2)} + \frac{\bar{C}_{1L} \bar{v}_{xL}}{\phi} \frac{\partial \ln \bar{\mu}_L}{\partial \bar{C}_{L1}} - (\frac{\bar{v}_{xL}}{\phi} - \bar{V}) + D_{Lt} \gamma_3 \right].$$

The terms on the left in Eq. (4.43) that are positive represent destabilizing effects and those that are negative represent stabilizing effects. Gravity is stabilizing when the displacement is downwards. The second term represents adverse mobility and can be re-expressed as

$$\frac{\bar{\mu}_L}{k_L} \bar{v}_{xL} - \frac{\bar{\mu}_G}{k_G} \bar{v}_{xG} = \bar{v}_{xG} \frac{\bar{\mu}_G}{k_G} [M - 1] + \frac{\bar{\mu}_L}{k_L} \phi c [\frac{1}{\rho_L} - \frac{1}{\rho_G}] \tag{4.44}$$

where the mobility ratio $M = \dfrac{k_G / \bar{\mu}_G}{k_L / \bar{\mu}_L}$ is expected to be large. Eq. (4.4) has been used and c is the net mass transferred across the front. Whereas $M - 1$ is positive and represents a destabilizing effect, the mass transfer effect is negative and constitutes a stabilizing effect. This effect arises out of the fact that a large volume of CO_2 dissolves in the oil to form a dissolved material of small volume. It causes the front velocity V to be less than $\bar{v}_{xG}$. Miller [Miller, 1975] found that such a term in steam condensation drives imparted a good amount of stability.

The other mass transfer terms, the last term in Eq.(4.43), have two positive contributions, in the terms $(-\dfrac{\partial \bar{C}_{L1}}{\partial x^*})$ and the denominator. The terms within the square brackets are analyzed by parts. In the first case, we assume that $\bar{\mu}_L$ is a constant. The term in square brackets in Eq. (4.43) then becomes $-[(\dfrac{\bar{v}_{xL}}{\phi} - V) - D_{Lt} \gamma_3][\dfrac{\rho_G k_G \alpha}{\phi \mu_G} + \dfrac{\rho_L k_L \alpha}{\phi \mu_L}]$. This term can be shown to be negative from Eq. (4.4) on using the fact that γ_3 is negative.

Hence it provides a stabilizing effect. This effect represents the fact that when a finger of CO_2 intrudes into oil, mass transfer depletes it. However, this procedure is effective only when the wavelength of interfacial disturbance is small, as it gives rise to a large area to volume (of the finger) ratio. Further, there can be conditions under which such disturbances can grow [Miller, 1978].

If in the third term on the left hand side of Eq. (4.43), we ignore the mass transfer contributions and keep only the effect of CO_2 on viscosity, a stabilizing effect is observed where the term denotes the fact that the adverse mobility ratio increases only gradually. This has been seen earlier [Cooney, 1966; Tan and Homsy, 1986] in miscible displacement. These three stabilizing mechanisms of mass transfer are shown schematically in Figure 4.2.

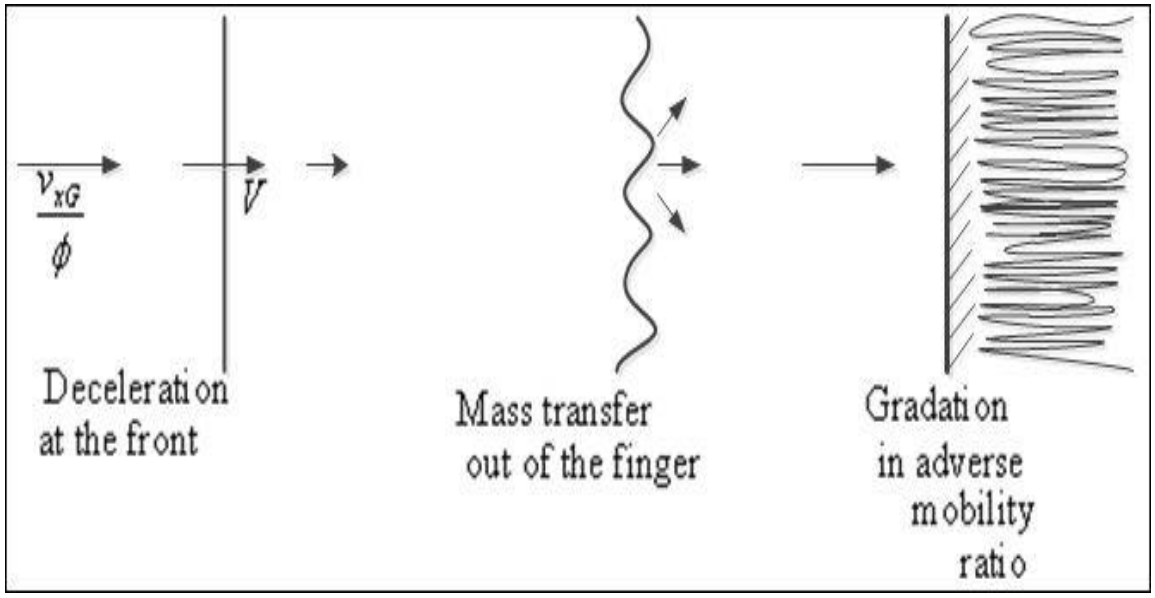

Figure 4.2. Three different mechanisms due to mass transfer that stabilize the process.

The main reason for undertaking this stability analysis is that previously, we have correlated the only full set of physical properties data [Tran et al. 2012] to be able to evaluate results of immiscible displacement by CO_2. We have looked at displacement in a single pore [Tran et al. under review] and much could be learned by using actual numbers in the results. To some physical properties given earlier, we add $k_L \sim k_G \sim 0.3\text{x}10^{-8}$ cm^2 and $\phi \sim 0.25$. The time is ½ year and the velocity of the front $V \sim 3.5\ \text{x}10^{-4}$ cm/s. The effect of CO_2 on viscosity of heavy crude as well as the viscosity itself (13.2 g/cm.s which unit = 1 Poise or 0.1 Pa.s) have been taken from the correlations of Tran et al [Tran et al. 2012] of the data by Chung et al. [1988). The specific volume of CO_2 in heavy oil of 1.06 cm^3/g reported there [Tran et al. 2012] has also been used. The value of the concentration gradient of CO_2 in oil has been approximated from Eq. (4.12) at $x^* = 0$ and worked out to $\frac{\partial \bar{C}_{L1}}{\partial x^*} \sim -0.73\, g/\text{cm}^4$. In addition, $\bar{C}_{L1} \sim$ 0.103 g/cm^3 and under the same conditions $\frac{\partial \ln \bar{\mu}_L}{\partial \bar{C}_{L1}} \sim$ -2.45 cm^3/mol.

The first term of Eq. (4.43) is gravity, and it was initially ignored. The second term was evaluated separately as two terms following Eq. (4.44). The first term there is the adverse mobility term and gave a very large destabilizing (positive) contribution ~ + $4\text{x}10^5$ (1 in Figure 4.3). The second term is the deceleration effect and gave rise to a large stabilizing effect ~ -$1.8\text{x}10^5$ (4 in Figure 4.3 and 1 in Figure 4.2). Both effects are independent of the wavenumber α and since the sum is positive, the deceleration effect is not sufficiently large to overcome the adverse mobility. The third term on the left in Eq.(4.43) was also broken into two parts as done earlier. The first term which did not have any variation of viscosity with CO_2, gave rise to a stabilizing effect of negligible

magnitude (2 in Figure 4.3 and 2 in Figure 4.2). Thus, the mass transfer effect of the finger formation is so small that it does not matter if it is positive or negative. The second part of the term represented the decrease of viscosity and gave rise to a strong negative (stabilizing) effect. This term goes to zero as α increases and to - ∞ as α goes to zero (3 in Figure 4.3 and 3 in Figure 4.2). The total (dashed line in Figure 4.3) is equal to zero at $\alpha_c \sim 0.531$ cm^{-1} or at a wavelength of 11.8 cm. Thus, wavenumbers smaller than 0.531 cm^{-1} (or wavelengths larger than 11.8 cm) are stable to infinitesimal fluctuations.

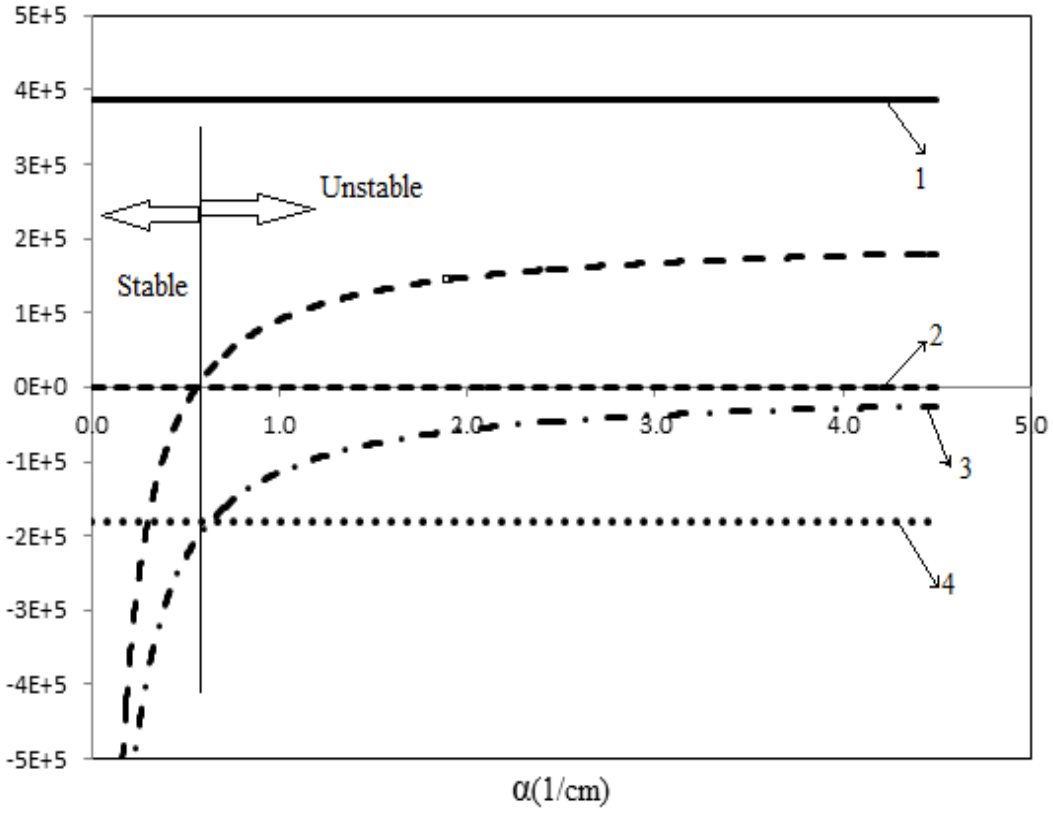

Figure 4.3. (1) represents adverse mobility ratio, the square dotted line (2) is the contribution of mass transfer, the dash-dot line (3) provides variation of viscosity, the round dotted line (4) is the effect of deceleration due to mass transfer, and the dashed line is the total, the critical where the total is zero.

The unstable disturbances which are of small wavelengths will give rise to a "mushy zone." Since the number for the term $\frac{\partial \ln \bar{\mu}_L}{\partial \bar{C}_{L1}}$ is very important to the present result, we report in brief how that quantity was obtained. Experimental data [Chung et al, 1988] was fitted to free volume theory [Tran et al. 2012] which gave us $\frac{\mu_L}{\mu_L(ref)}$ as a function of CO_2 concentration, temperature and pressure. On differentiating the logarithm of this term to get $\frac{\partial \ln \bar{\mu}_L}{\partial \bar{C}_{L1}}$, the effect of the reference viscosity is lost. That is, the base oil viscosity does not play a role as long as the oil is heavy that free volume theory can be applied.

It should be pointed out that here, and in studies of miscible displacements [Cooney, 1966; Tan and Homsy, 1986], the results are dependent on the concentration profiles. However, with some care, it can be shown that one of them [Tan and Homsy, 1986] at zero time, provides a marginal stability and in our notations

$$\alpha_c = -\frac{\bar{C}_{L1}}{4}\frac{\partial \ln \bar{\mu}_L}{\partial \bar{C}_{L1}} \tag{4.45}$$

which draws attention to the importance of concentration dependence on viscosity. We also evaluate this α_c as 0.063 cm^{-1}.

It is now possible to examine the case where the partition coefficient m_1 is very high making $\bar{C}_{1L}$ very low. The last term in Eq. (4.43) simplifies a great deal and becomes positive and proportional to $-\frac{\partial \bar{C}_{L1}}{\partial x^*}/\bar{C}_{1L}$ at the interface. This ratio is also found to be positive but inversely proportional to $\sqrt{t}$ where Eq. (4.8) and the boundary conditions have been used. Consequently, as the solubility decreases the range of

instability that is confined to small wavelengths, increases and reaches infinity when the solubility drops to zero.

It is not possible to observe the displacement process in the laboratory using heavy oil because of the very small rates involved. Some related cases can be analyzed. Displacement of brine in sandstone by CO_2 has been studied by Ott et al. [2012] using x-ray tomography. A key ingredient in the form of a decrease in the viscosity of the displaced fluid with increased carbonation, is missing. In their experiments, they do not observe a sloping front that would imply unstable modes at large wavelengths but instead show a mushy zone. Wellington and Vinegar [1988] report using tomography that the displacement with CO_2 is strongly compromised in their cores by gravity override, which disappears when CO_2 foams are used. However, a careful examination reveals viscous fingering at large times and at small wavelengths, even though gravity override is not seen. Rojas and Ali [1988] have looked at displacement of heavy oils by CO_2 in a sand pack and observe better displacement with increasing CO_2 pressures till miscibility. They attribute this increase mainly due to the decrease in oil-CO_2 surface tension, which they measure as well. No effect of instability is seen.

Observations from other systems also exist, namely the miscible systems, which yields some information on immiscible systems. Perrine [1963], for miscible displacements with $M < 17$, made some seeming conflicting observations on core studies. Almost all cases examined showed unstable displacements. Perrine also observed that the displacement appeared to move like that predicted by the Buckley-Leverett scheme which is suited to immiscible displacement. Since the oil used was light, the critical wavelength is small. The disturbances of wavelengths below this which are unstable can

only provide a mushy zone, and the movement may well be represented approximately by the Buckley-Leverett scheme.

Finally, if we return to the gravity term in Eq. (4.43) then the effect of allowing the full term as a stabilizing effect ~ +1000, which will be seen in gravity assisted drainages, it does not affect the value of α_c significantly.

We have broadened the scope in the present analysis to include all mechanisms that lead to stability/instability in the displacement process, that is, provided a general formulation which includes features from both immiscible and miscible displacements. One important contribution made is that if we look at the numerical results based on physical properties data some mechanisms, the first two in Figure 4.2, drop out and the one that turns out to be important, the last one in Figure 4.2, is the one not considered in immiscible displacement.

5. CONCLUSION AND RECOMMENDATION

There are some important of results that accomplished in this study. First of all, with free volume theory, it is possible to correlate both thermodynamic and transport properties of heavy oil - CO_2 systems using parameters that are physically meaningful. The results are based on only one set of experimental data that are extensive and contain all the necessary values for the physical properties. The formulation is in the form of fractional change. Thus an exciting possibility exists that the correlation from free volume theory can be transferred to other heavy oils from the one study here. These data on swelling, and has been correlated with Welker and Dunlop equation, and this equation has been justified here using free volume theory, which also forecasts that the diffusivity of CO_2 in heavy oils is strongly dependent on the CO_2 concentration.

Second, study of multiphase flows in a single pore between CO_2 - heavy oil with mass transfer between two phases. The net effect of concentration dependent viscosity and diffusivity are low because of adverse effects of convection noted here for the first time, which limit CO_2 penetration into the oil. The pressure drop is dominated by surface tension and lowering surface tension will improve the displacement process, hence the recovery of oils improve, as conducted the film thickness left behind is determined by viscocapillary effects at larger capillary numbers but which thickness (and retention), decreases on carbonation. At small capillary numbers, it is dominated by the disjoining pressures, where the film thickness is larger than those predicted by viscocapillary effects. Fluid mechanics prevailed at large capillary number. Because the viscosity of the oil ahead of the front is not reduced, we need better solvents such as naphtha.

Third, the displacement front in CO_2 displacing heavy crude can be stabilized by mass transfer, and it is the reduction of viscosity by carbonation of oil that provides the key stabilizing mechanism where the adverse mobility ratio increases gradually ahead of the front instead of in a step. However, the disturbances of small wavelengths are unstable and will lead to a mushy zone. Gravity drainage by itself is not able to overcome the destabilizing effect of an adverse mobility ratio of this magnitude. Displacement of lighter oils with no miscibility, is more stable than the displacement of heavy oils where the CO_2 solubility is very low, which is more unstable.

For future research:

1. One can follow Chung et al. (1988) to design an experimental procedure set-up and carry out to establish complete set of physical properties data for CO_2-heavy oil mix with oils from different sources. The free volume theory is in form of fractional change and independent of oil type because of that more experimental data need.
2. Design an experimental procedure using single molecular microscopic imaging instruments available to investigate the displacement by CO_2 of oil in a pore with micro-channel and nano - channel.
3. Design an experimental procedure using Computerized Tomography instruments available to investigate the moving front and flow behavior of CO_2 in cores and sandpacks, displacing heavy oils. This would tell us the nature of the stability in these systems.

APPENDIX

Section 2.

To determine the surface tension, consider the chemical potentials. For the solvent (1)

$$\mu_1 = \mu_1^o + RT \ln \phi = \mu_1^{os} + RT \ln \phi_1^s - \gamma a_1 \qquad \text{(A.1)}$$

where the size of oil molecules have been considered to be very large compared to that of CO_2, and the interaction energy between them is negligible. The chemical potential in the bulk is equal to that at the surface, where surface quantities carry a superscript *s*. Further, γ is the surface tension of the mixture and a1 is the partial molar area, which is assumed to be a constant and equal to the pure property below. When the oil is pure, we substitute $\phi = 1$ and $\phi_1^s = 1$, leading to

$$\mu_1^{os} = \mu_1^o + \gamma_1 a_1 \qquad \text{(A.2)}$$

Substituting into Eq. (A.1) and rearranging

$$\phi_1^s = \phi_1 . \exp\left[\frac{(\gamma - \gamma_1) a_1}{RT} \right] \qquad \text{(A.3)}$$

is obtained.

Similarly, for the solute (2)

$$\mu_2^{\infty} + RT \ln \phi_2 = \mu_2^{\infty s} + RT \ln \phi_2^s - \gamma a_2 \qquad \text{(A.4)}$$

where the superscript ∞ stands for infinite dilution, which is used to cover systems above the critical temperature of the solute as well. Rearranging,

$$\phi_2^s = \phi_2 H_s \exp \frac{\gamma a_2}{RT} \qquad \text{(A.5)}$$

where $H_s = \frac{\mu_2^{\infty} - \mu_2^{\infty s}}{RT}$. Changing notations to $\phi_1 = 1-\phi;\ \phi_1^s = 1-\phi^s;\ \phi_2 = \phi;\ \phi_2^s = \phi^s$ and on adding Eqs. (A.3) and (A.5)

$$1 = \phi H_s . \exp(\gamma a_2 / RT) + (1-\phi) . \exp[(\gamma - \gamma_1) a_1 / RT] \qquad \text{(A-6)}$$

is obtained. This has been used as Eq. (2.31) in the text in section 2.

BIBLIOGRAPHY

Amaefule, J.O., and Handy, L.L, "The effect of interfacial tensions on relative oil/water permeability of consolidated porous media," *SPE J*., 22, 371 (1982).

Bercic, G. and Pintar, A, "The role of gas bubbles and liquid slug lengths on mass transport in the Taylor flow through capillaries," *Chem. Eng. Sci.,* 52, 3709-3719 (1997).

Berry, G.C. and Fox, T.G, "The viscosity of polymers and their concentrated solutions," *Adv. Polymer Sci*., 5, 261-357 (1968).

Bird, R.B., Stewart, W.E., Lightfoot, E.N, *Transport Phenomena,* 2nd ed., John Wiley and Sons, N.Y., p. 31, 864 (2002).

Brackbill, J.U, Kothe, D.B and Zemach, C, "A continuum method of modeling surface tension," *J. Comp. Physics*., 100, 2, 335-354 (1992).

Brelvi, S. W. and O'Connell, J.P, "Generalized isothermal equation of state for dense liquids," *AIChE J*., 21, 171 (1975).

Bretherton, F.P, "The motion of the long bubbles in tubes," *J. Fluid mech*.,100, 166-188 (1961).

Chang, Y.-B., Coates, B.K., Nolen, J.S, "A compositional model for CO2 floods including CO2 solubility in water," *SPE Res. Eval. Eng*.,1, 155 (1998).

Chang, H.-C., "Stability of fluid-fluid displacement with mass transfer in porous media: A model for carbon dioxide flooding of oil fields," MS Thesis, Department of Chemical Engineering, University of Missouri-Rolla (1983).

Chuoke, R.L., van Meurs, P., and van der Poel, C, "The Instability of Slow, Immiscible, Viscous Liquid-Liquid Displacements in Permeable Media," *Trans. AIME Pet Eng*., 216: 188-194 (1959).

Cohen, M.H., Turnbull, D, "Molecular transport in liquids and glasses," *J. Chem. Phys.*, 31, 1164 (1959).

Cooney, D.O, "Effect of mass transfer on the stability of miscible displacement fronts in porous media," *I&EC Fundam* 5: 426. (1966).

Chung, F.T.H., Jones, R.A., and Nguyen, H.T, "Measurements and correlations of physical properties of CO2/ heavy-crude-oil mixtures," *SPE Res. Eng*., 3, 822 (1988).

Craig, F.F. Jr, *The Reservoir Aspects of Waterflooding*, SPE Dallas, TX (1971).

Crank, J. and Park, G.S, Methods of measurement, Diffusion in Polymers, J. Crank and G.S. Park, eds.; Academic Press, p. 1 (1968).

Derjaguin, B.V, "Theory of capillary condensation and other capillary phenomena considering the disjoining action of semimolecular liquid surfaces," *Zh. Fiz. Khim.*, 14, 137 (1940).

Dzyaloshinskii, I.E.,Lifshitz, E.M. and Pitaeveskii, L.P, "van der Waals forces in liquid films," *Soviet Phys. JETP*., 10, 161 (1960).

Foster, W.R, "A low-tension waterflooding process," *SPE J*., 25, 205-210 (1973).

Frumkin, A, "Phenomena of wetting and adhesion of bubbles, I," *Zh. Fiz. Khim*., 12, 337 (1938).

Fujita, H, "Diffusion in polymer-diluent system," *Adv. Polymer Sci.*, 3, 1 (1969).

Giavedoni, M.D and Saita, F.A, "The axisymmetric and plane cases of a gas phase steadily displacing a Newtonian liquid – a simultaneous solution of governing equations," *Phys. Fluids*., 9, 2420 (1997).

Green, D. W., and Wilhite, G.P, *Enhanced Oil Recovery*, SPE Dallas, TX (1998).

Gupta, R., Flecture, D.F., Haynes, B.S. "On the CFD modeling of Taylor flow in microchannels," *Chem. Eng. Sci*., 64, 2941 (2009).

Hagoort, J, "Displacement Stability of Water Drives in Water-Wet Connate-Water-Bearing Reservoirs," *SPE J* 14: 63 (1974).

Haward, R.N, *The Physics of Glassy Polymers*, Applied Science, London (1973).

Heil, M, "Finite Reynolds number effects in Bretherton problem," *Phys. Fluids*., 13, 2517-2521 (2001).

Helba, A.A., Sahimi, M., Scriven, L.E., and Ted Davis, H, "Percolation theory of two-phase relative permeability," *SPE Res Eng*., 7, 123 (1992).

Hirasaki, G.J., Yang, S.Y. "Dynamic contact line with disjoining pressure, large capillary numbers, large angles and pre-wetted, precursor, or entrained films": Con*tact Angle, Wettability and Adhesion 2*; K. Mittal, ed.; VSP, 1-30 (1993)

Huang, Y.H. and O'Connell, J.P, "Corresponding states correlation for the volumetric properties of compressed liquids and liquid mixtures," *Fluid Phase Equilibria*.,37, 75 (1987).

Hughes, G.R., Rao, N.D, "Current research and challenges pertaining to CO2 flood and sequestration,"http://www.spe.org/twa/print/archives/2011/2011v7n2/09Academia_TWA_v7n2.pdf. Oct 16, 2014.

Hutchinson, Jr. C.A., and Braun, P.H, "Phase relations of miscible displacement in oil recovery," *AIChE J.*, 7, 64-72 (1961)

Issever, K., Pamir, A.N., and Ali, T, "Performance of Heavy – Oil field under CO2 injection, Bati Raman, Turkey," *SPE Res. Eng.*, 8, 256 (1993).

Kang, S., Gao,C., and Zhang, S, "Scientific Research and Field Application of CO2 immiscible flooding in heavy oil recovery," Paper presented at SPE enhanced oil recovery conference, Kuala Lumpur, malaysia, july 2013, SPE 165210 (2013).

Kim,J.S., Dong, Y., and Rossen, W.R, "Steady state flow behavior of CO2 foam," *SPE J.*, 10, 405 (2005).

Kirkwood, J.G, "Critique of the free volume theory of the liquid state," *J. Chem. Phys*., 18, 380 (1950).

Kreutzer, M.T., Kaptejin, F., Moulijn, J.B., Klein, C.R and Heiszwolf, J.J, "Inertial and interfacial effects on pressure drop of Taylor flow in capillaries," *AIChE J.*, 51, 2428-2440 (2005).

Kulkarni, S.S. and Stern, S.A, "The diffusion of CO2, CH4, C2H4 and C3H8 in polyethylene at elevated pressures," *J. Polym. Sci. Polym. Phys. Ed*., 21, 441 (1983).

Larson, R.G, Ted Davis, H, and Scriven, L. E, "Displacement of residual nonwetting fluid from porous media," *Chem. Eng. Sci.*, 36, 75 (1981).

Lake, L.A., Enhanced Oil Recovery. Prentice-Hall, NJ, p. 268 (1988). See also Arya, A., Hewett, T.A., Larson, R.G., and Lake, L.W, "Dispersion and Reservoir Heterogeneity," *SPE Reservoir Eng.*, 3: 139 (1988).

Lake, L.W, *Enhanced Oil Recovery*, Prentice-Hall, N.J., p. 268 (1989).

Lake, L.W, "Reservoir description: Key to success in chemical-enhanced oil recovery. Surfactant-Based Mobility Control, ACS Symp," Series, ACS, Washington, D.C., p. 53 (1988).

Melrose, J.C., and Brandner, C.F, "The role of capillary forces in determining microscopic displacement efficiency for oil recovery by waterflooding," *J. Canad. Pet. Tech.*, 13, 54 (1974).

Miller, C.A., Neogi, P, *Interfacial Phenomena, Static and Dynamic Aspects*. 2nd ed. Boca Raton, FL: CRC Press, 421 (2008).

Miller, C.A, "Stability of Moving Surfaces in Fluid Systems with Heat and Mass Transport III. Stability of Displacement Frots in Porous Media," *AICHE J.*, 21: 474 (1975).

Miller, C.A. and Neogi, P, *Interfacial Phenomena: Equilibrium and Dynamic Aspects*, CRC Press, Inc., p. 36-40, see also problem 1.14 on p. 56-57. (2008).

Morrow, N.R, *Interfacial Phenomena in Oil Recovery*. New York, NY: Marcel Dekker (1991).

Mulliken, C.A., Sandler, S.I, "The prediction of CO2 solubility and swelling factors for enhanced oil recovery," *IEC Process Des. Dev.*, 19, 709 (1980).

Muskat, Morris., *Physical Principles of Oil Production*, McGraw-Hill Book Co.: New York (1949).

Neogi, P., "Oil Recovery and Microemulsions", in *Microemulsions: Structure and Dynamics*, S.E. Friberg and P. Bothorel, eds.; CRC press 197, Boca Raton, Florida (1987)

Outmans, H.D, " Nonlinear Theory for Frontal Stability and Viscous Fingering in Porous Media," *Soc. Pet. Eng 1*: 165-176 (1962).

Paracello, V. P., Bartosek, M., de Simoni, M, "Experimental evaluation of CO2 injection in heavy oil Reservoir," Paper presented in the international Petroleum Technology conference, Bangkok, Thailand, Feb. 2012, IPTC 14869 (2001).

Perkins, T.K. and Johnston, O.C, "A Study of Immiscible Fingering in Linear Models," *Soc. Pet. Eng. J* 1: 39-45 (1969).

Perrine, R.L, "A unified theory of stable and unstable miscible displacement," *SPE J.*, 3: 205 (1963).

Prausnitz, J.M., Lichtenthaler, R.N., de Azevedo, E.G., *Molecular Thermodynamics of Fluid Phase Equilibrium*, 3rd ed., Prentice-Hall, Inc., Englewood Cliffs, N.J., p.607 (1999).

Rachford, H.H. Jr., "Instability in Water Flooding Oil from Water-Wet Porous Media Containing Connate Water," *Trans. AIME.*, 231: 133-148 (1964).

Reamer, H.H. and Sage, B.H, "Phase Equilibria in Hydrocarbon Systems. Volumetric and Phase Behavior of the n - Decane – CO2 system," *J. Chem. Eng*. Data 8: 508 (1963).

Reed, R.L., and Healy, R.N, "Some physic-chemical aspects of microemulsion flooding": a review. *Improved Oil Recovery by Surfactant and Polymer Flooding*, D.O. Shah and R.S. Schechter, eds., Academic Press, New York, p. 383 (1977).

Rojas, G.A and Ali, S.M.F, " Dynamics of subcritical CO2/brine floods for heavy oil recovery," *SPE Res. Eng*., 3, 35-44 (1988).

Sabbagh, H., Eu, B.C, "Generic van der Waals equation of state for polymers, modified free volume theory, and the self-diffusion coefficient of polymeric liquids," *Physica A*., 389, 2325 (2010).

Saffman, P.G. and Taylor, G.I, "The Penetration of a Fluid into a Porous Medium or Hele-Shaw Cell Containing a More Viscous Liquid," *Proc. R. Soc. Lond* A245 (1242): 312-329 (1958).

Scheidegger, A.E, "On the Stability of Displacement Fronts in Porous Media: A Discussion of the Muskat-Aronofsky Model," *Can. J. of Physics*., 38: 153-162 (1960).

Slattery, J.C, "Interfacial effects in the entrapment and displacement of residual oil," *AICHE J*., 20, 1145 (1974).

Slattery, J.C., *Advanced Transport Phenomena,* Cambridge University Press (1999).

Smith, D.H., Surfactant-Based Mobility Control. ACS Symposium Ser. 373, ed., ACS Washington, D.C.(1988).

Simon, R., and Graue, D.J, "Generalized correlations for predicting solubility, swelling and viscosity behavior of CO2-crude oil system," *J. Pet. Soc*. 17, 102 (1965).

Stegemeier, G. L, "Mechanisms of entrapment and mobilization of oil in porous media," *Improved Oil Recovery by Surfactant and Polymer flooding*, D. O. Shah and R. S. Schechter, eds., Academic Press, New York, p.55 (1977).

Tharanivasan, A.K., Yang, C. and Gu, Y, "Measurements of molecular diffusion coefficients of carbon dioxide, methane, and propane in heavy oil under reservoir conditions," *Energy & Fuels*., 20, 2509 (2006).

Teletzke, G.F., Davis, H.Ted and Scriven, L.E, "Wetting hydrodynamics," *Review Phys. Appl.*, 23, 989-1007 (1988).

Tran, T., Neogi, P., Bai, B, "Free volume estimates of thermodynamics and transport properties of heavy oils with CO_2," *Chemical Engineering Science*., 80, 100(2012).

Tran, T., Ahmad, M.A., Neogi, P and Bai, B, "A single pore model of displacement of heavy crude oil by carbon dioxide," under review (2014).

USGS. Heavy oil and natural bitumen-strategic resources. Fact Sheet FS – 070-03, August, 2003. Pubs.usgs.gov.fs/fs070-03/fs070-03.html.

van Baten, J.M and Krishna, R, "CFD simulations of mass transfer from Taylor bubbles rising in circular capillaries," *Chem. Eng. Sci.*, 59, pp. 2355-2545 (2004). Corrigendum. *Chem. Eng. Sci.,* 59, 4941 (2011).

Vrentas, J.S., Duda, J. L, "Molecular diffusion in polymer solution," *AIChE J.*, 25, 1 (1979).

Watson, K.M., Nelson, E.F., Murphy, G.B, "Characterization of petroleum fractions," *Ind. Eng. Chem.*, 27, 1460 (1935).

Welker, J.R., Dunlop, D.O, "Physical properties of carbonate oils," *J. Pet. Tech.*, 15, 873 (1963).

Wellington, S.L., and Vinegar, H.J., "Surfactant-Induced Mobility Control for Carbon Dioxide Studied with Computerized Tomography". In *Surfactant-Based Mobility Control*, ed. D.H. Smith, ACS Symposium Series, p. 344 (1988).

Wesseling, P., Principles of Computational Fluid Dynamics, Springer, (2001).

Yang, C., Gu, Y, "A new method for measuring solvent diffusivity in heavy oil by dynamic pendant drop shape analysis (DPDSA)," *SPE J.*, 11, 48 (2006)

Yang, C. and Gu, Y, "Diffusion coefficients and oil swelling factors of carbon dioxide, methane, ethane, propane, and their mixtures in heavy oil," *Fluid Phase Equilibria*., 243, 64 (2006).

Yang, D., Gu, Y, "Determination of diffusion coefficients and interface mass transfer coefficients of the crude oil-CO2 system by analysis of the dynamic and equilibrium interfacial tension," *Ind. Eng. Chem. Res*., 47, 5447 (2008).

Zhang, Y.P., Hyndman, C.L. and Maini, B.B, "Measurement of gas diffusivity in heavy oils," *J. Pet. Sci. Eng.*, 25, 37 (2000).

VITA

Truynh Tran enrolled in the Chemical and Biochemical Engineering Program at the Missouri University of Science and Technology in the fall of 2007. He graduated with the Bachelor of Science in Chemical Engineering degree in May, 2010. He accepted and received the funding for studying his graduate education in the Chemical Engineering Program from the Missouri University of Science and Technology, starting from the fall of 2010. He received his Master of Science in Chemical Engineering degree in 2013. In December, 2014, he was awarded the Doctor of Philosophy degree in Chemical Engineering at the Missouri University of Science and Technology (Rolla, Missouri, USA).